Marco António Cavaco Rodrigues

Bachelor in Engineer of Micro and Nanotechnologies

Design and simulation of a direct and indirect drive electrostatically actuated resonant micro-mirrors for scanner applications

Dissertation submitted in partial fulfillment of the requirements for the degree of

Master of Science in Micro and Nanotechnologies Engineering

Adviser: Dr. Ivan Grech, Associate Professor, Department of Microelectronics & Nanoelectronics of the University of Malta

Co-Adviser: Dr. Luís Pereira, Associate Professor, Faculty of Sciences and Technology New University of Lisbon

Examination Committee

Chairperson: Dr. Hugo Águas

Raporteurs: Dr. Manuel Mendes

Dr. Luís Pereira

FACULDADE DE CIÊNCIAS E TECNOLOGIA
UNIVERSIDADE NOVA DE LISBOA

September, 2018

Design and simulation of a direct and indirect drive electrostatically actuated resonant micro-mirrors for scanner applications

“Aprenda como se fosse viver para sempre,
viva como se fosse morrer amanhã” – Santo Isidoro de Sevilha

Acknowledgments

Over the last years of my academic path I have been trying to pursue knowledge in the MEMS (micro-electrical-mechanical-systems) field, as soon as I was reaching the time of doing this dissertation I was pretty sure I wanted to do something on it. Because of that, I would like to first thank my adviser Prof. Ivan Grech, to let my dream come true, by accepting me to work in the Department of Microelectronics & Nanoelectronics of the University of Malta, with the amazing proposal on resonant micro-mirrors. During my stay in this beautiful island, he was available every week to help and guide me, beside his huge amount of work.

There are also two amazing mentors that helped me through this path. I would like to thank Eng. Barnaby Portelli and Eng. Russell Farrugia from DMN/UM, for sharing their huge knowledge in the most diverse fields, starting on Engineering and finishing on History. They were also a key to go deeper inside the Maltese culture, by sharing places, routes and events that otherwise I would have missed. Thank you also for the road trip in the harmonious island of Gozo, without you I couldn´t have experienced half of it. I would like to give one last special thanks to Eng. Russell Farrugia for being so supportive with me, your help couldn´t be more commendable, starting to borrow me your tent and eventually getting me a job.

From outside the University, I would like to thank my flatmates Kristine and Victor, for being the perfect couple to live with, and for helping me to improve both my English and Spanish. To the staff of Café Riche, for let me work as a waitress occasionally. To Iacopo, Valeria, Ana, Irene and all the other amazing people that I met there, and shared with me the beauty of this moving organism called Malta, in which we could live in almost perfect symbiosis.

Gostaria de agradecer ao meu co-orientador Prof. Luís Pereira da FCT/UNL, por apoiar e icentivar a minha aventura neste ramo, que em muitos aspectos difere dos conteúdos leccionados ao longo do percurso académico. Um sincero obrigado, não só por ter inaltecido o gosto por estes dispositivos através das suas aulas, como também a confirmar que seria este o caminho a tomar quando chegasse a hora da dissertação.

Um gigante abraço à minha familia, começando pelos meus pais que sempre me apoiram e inicialmente me canalizaram para as micro e nanotecnologias, por todo o esforço económico subjacente e por todas as chamadas de telefone que enterropiam o meu estudo e que foram essencias para descarregar algum stress acumulado e ter forças para continuar, por toda a icentivação a explorar territórios desconhecidos e por me terem enraizado um espirito aventureiro e lutador, que para tudo quero continuar a utilizar. Obrigado aos meus avós por me

alojarem durante os anos de faculdade, por me aturarem e mesmo assim mimarem. Aos meus pequenos irmãos David e Viviana, por me fazerem lavagens cerebrais sempre que ia casa e lembrarem-me que apesar de todo o estudo e trabalho ainda posso descer à idade deles. Um agradecimento a toda a restante familia por todo o carinho e apoio indespensável.

Obrigado aos meus colegas gurus Miguel Alexandre, João Pina, Miguel Ramos, André Moura e outros tantos por me auxiliarem em todos e quaisquer trabalhos nos quais eventualmente bloqueasse. Ao Kevin e ao Pedro por me hospedarem sempre que havia festas da FCT e me tinha de deslocar entre margens. Ao Nuno Lima por ser o meu companheiro de barco e pelas conversas que curavam o enjoo quando o tejo estava atribulado. Ao Xavier pelo seu sentido de humor arrojado e por me regalar com excelentes gargalhadas acompanhadas de choro. Á Catarina Rijo por horas a fio a observar um computador em busca de motivação para trabalhos. Ao Nuno Ferreira por ser um ser de extrema inteligéncia e me regalar com rap criolo. Ao Ricardo, à Carolina, ao Tomás, ao Casa Branca por excelente trabalho de equipa sempre acompanhado de muito boa disposição. À Laura Serrano, ao Manuel, ao Sérgio, ao Zé, ao Miguel, ao Filipe e a todos os outros que fizeram desta viagem de comboio TGV extremamente aplativa e enriquecedora.

Um genuino obrigado ao Prof. Dr. Rodrigo Martins e à Prof. Dra. Elvira Fortunato pela criação, promoção do curso de Engenharia de Micro e Nanotecnologias.

Um abraço profundo a todas as pessoas e amigos que me acompanharam fora do âmbito da faculdade. Ao Vasco, ao Tito à Ana e ao J.P por terem crescido comigo e por terem estimulado a minha mente ao longo de todos estes anos. Ao Topê, pelas noites e dias insanos em Lisboa, que dariam narrativas surrealistas, pela ajuda emocional e pelo riso interminável de sol a sol. Ao David por ser um tipo porreiro de ERASMUS que me ensinou muito sobre o meu próprio País. Ao Gonçalo e ao Bernardo, por estimularem o outro hemisfério do meu cérebro. Ao Melinho por me proporcionar histórias incriveis e me embarcar em noites de outras gerações. À Laura por despertar em mim um lado espiritual há muito esquecido e por me fazer lembrar que engenharia pode caminhar de braço dado com ele.

A lumped thank you to everyone, inside and (a lot) outside of this list, this dissertation was made by all of you.

Abstract

Laser scanners have been an integral part of MEMS research for more than three decades. The demand for electrostatically actuated scanning micro-mirrors have been growing in the last decade, mainly for pico-projection and medical applications. These type of actuation wins over others, because it provides long-term stability, size advantages and fabrication schemes which are easier to render CMOS compatibility.

The growing field in softwares capable of design and simulate MEMS devices, have been a crucial help for engineers, which are limited to a few of them and still cost huge amount of time. *MEMS+*® is a software platform that provides simulation results up to 100 times faster than conventional finite element analysis tools and allows to integrate designs in *MathWorks*®.

In this work two types of electrostatically actuated scanning micro-mirrors were designed and simulated using both *MEMS+*® and *MathWorks*®, one is a direct drive micro-mirror and the other an indirect drive micro-mirror. In the first the torque is imparted directly from the actuation mechanism to the frame containing the mirror, and in the second the resonance mode amplifies a small motion in a larger mass to a considerably larger motion in the smaller mirror. Regarding the direct-drive micro-mirror, the presented work mainly shows the reliability of *MEMS+*® compared to other softwares. The indirect drive one, is a state-of-art solution for high frequency electrostatically actuated micro-mirrors, and all the simulations taken on it were aimed to verify it´s behaviour, and then proceed with the microfabrication step. The target microfabrication technology is SOIMUMPs.

Keywords: Scanning micro-mirror, electrostatically actuated, *MEMS+*®, direct drive, indirect drive, SOIMUMPs.

Resumo

Scanners de laser têm sido uma parte integral dos dispositivos MEMS há mais de três décadas. A procura por micro-espelhos resonantes electroestaticamente atuados tem crescido na última década, essencialmente para aplicações médicas e de pico-projeção. Este tipo de atuação electrostática ganha em relação a outras, pois permite estabilidade a longo prazo, tem vantagens em termos de tamanho, e os esquemas de fabricação são mais fáceis de conceber e compatíveis com tecnologia CMOS.

O crescimento do ramo de softwares capazes de desenhar e simular MEMS, tem sido uma ajuda crucial para os engenheiros que estão ainda limitados a poucos e que demoram muito no que toca a certas simulações. O *MEMS+*® é um software que permite resultados de simulações 100 vezes mais rápidas que os softwares convencionais, e permite a integração com *MathWorks*®.

Neste trabalho dois tipos de micro-espelhos electroestaticamente atuados foram desenhados e simulados usando tanto o *MEMS+*® como o *MathWorks*®, um destes micro-espelhos é acionado diretamente e o outro indiretamente. No primeiro, o torque é acionado diretamente pelo mecanismo de atuação, no segundo, o modo de ressonância amplifica um pequeno movimento numa parte do dispositivo de maior massa e esta por sua vez amplifica o um maior movimento no próprio espelho. No que diz respeito ao micro-espelho diretamente acionado, o presente trabalho foca-se em mostrar a fiabiliadade do *MEMS+*® em relação a outros softwares. O micro-espelho indiretamente acionado é uma abordagem de estado-de-arte, no que toca a micro-espelhos de alta frequência electroestaticamente atuados, e as simulações empregues no mesmo foram focadas em verificar se o seu comportamento seguia as especificações e assim poder-se proceder para a sua microfabricação e posterior comercialização. O processo de microfabricação em questão é o SOIMUMPs.

Palavras-chave: Scanners de laser, electroestaticamente atuado, *MEMS+*®, acionado diretamente, acionado indiretamente, SOIMUMPs.

List of Abbreviations

AVC	Angular Vertical Combs
CMOS	Complementary Metal-Oxide-Semiconductor
DMD	Digital Micro-mirror Device
DMN/UM	Department of Microelectronics & Nanoelectronics of the University of Malta
DRIE	Deep Reactive Ion Etching
FEM	Finite Element Method
HPB	Half-Power Bandwidth
LCoS	Liquid Crystal on Silicon
MEMS	Micro-Electromechanical Systems
MUMPs	Multi-User MEMS Processes
NEMS	Nano-Electromechanical Systems
PSG	Phosphosilicate Glass
RIE	Reactive Ion Etching
SLM	Spatial Light Modulators
SVC	Staggered Vertical Combs
SOI	Silicon-On-Insulator
UV	Ultraviolet

List of Symbols

A_0	Common Area between Plates
α	Alpha Rayleigh Damping
β	Beta Rayleigh Damping
ζ	Modal Damping
ε	Permittivity of the Medium
ε_0	Absolut Permittivity
ω_0	Angular Resonant Frequency
θ_{MMSA}	Maximum Mechanical Scan Angle
$[C]$	Damping Matrix of the System
$[K_s]$	Stiffness Matrix of the System
$[M]$	Mass Matrix of the System
$M(\theta)$	Torque
f_0	Resonant Frequency
K_s	Torsional Stiffness
l_0	Finger´s Length
I_m	Mass Moment of Inertia
x_0	Finger´s Initial Overlap

Table of Contents

ACKNOWLEDGMENTS ..... **VII**

ABSTRACT ..... **IX**

RESUMO ..... **XI**

LIST OF ABBREVIATIONS ..... **XII**

LIST OF SYMBOLS ..... **XIV**

TABLE OF CONTENTS ..... **XVI**

LIST OF FIGURES ..... **XVIII**

LIST OF TABLES ..... **XXI**

MOTIVATION ..... **XXII**

OBJECTIVES ..... **XXIII**

CHAPTER 1: INTRODUCTION **1**

1. RESONANT MICRO-MIRRORS **1**

1.1. LASER SCANNING FOR PICO-PROJECTION 1

1.2. ACTUATION PRINCIPLE: ELECTROSTATIC 2

1.3. DESIGN TECHNIQUES 5

1.4. DIRECT AND INDIRECT DRIVE 6

1.1. DYNAMIC BEHAVIOUR 6

2. TARGET PROCESS: SOIMUMPS **9**

3. *MEMS*+® **10**

CHAPTER 2: DIRECT DRIVE MICROMIRROR **11**

1. PROCESS AND MATERIALS **11**

2. DESIGN **12**

3. EXTRACTING QUALITY FACTOR AND RAYLEIGH DAMPING **15**

3.1. Q FACTOR'S EXTRACTION USING HPB FORMULA 15

4. SIMULATION AND RESULTS **16**

4.1. MODAL ANALYSIS 16

4.1.1. Results of the Modal Analysis *16*

4.2. FORCE AND DC SWEEP ANALYSIS 17

4.2.1. Results of the Force Sweep Analysis *18*

4.2.2. Results of the DC sweep analysis *19*

4.2.3. Comparing both MEMS+® and CoventorWare® *19*

4.3. FREQUENCY RESPONSE 20

4.3.1. Frequency response at different timespans *20*
4.3.2. Frequency response at different numerical configurations *21*
CHAPTER 3: INDIRECT DRIVE MICROMIRROR **23**
1. DESIGN **23**
2. EXTRACTING Q FACTOR AND RAYLEIGH DAMPING **24**
2.1. Q FACTOR'S EXTRACTION USING *COVENTORWARE*® 24
2.2. OBTAINING RAYLEIGH DAMPING ALPHA 26
2.3. OBTAINING RAYLEIGH DAMPING BETA 27
3. SIMULATION AND RESULTS **28**
3.1. MODAL ANALYSIS 28
3.2. FREQUENCY RESPONSE 29
3.2.1. Frequency response with different Comb-drives *29*
3.2.2. Frequency for different voltages *31*
3.2.3. Optimization: Changing spring's length *32*
3.2.4. Obtaining the Amplification Factor *32*
3.2.5. Final Frequency Response and Phase *33*
3.2.6. MATLAB® and Simulink® Comparison *35*
CHAPTER 4: CONCLUSION **36**
REFERENCES **39**
ANNEXES **42**
A. SOIMUMPS` MICROFABRICATION STEPS **42**
B. *MEMS*+® TABS AND MATERIAL DATABASE **44**
C. *MATLAB*® SCRIPTS **47**

List of Figures

Figure 1 – Raster scanning architecture where each mirror is responsible for each axis. Adapted from [6].....1

Figure 2 – Comb-drive designs: a) Lateral Combs; b) Rotary Combs; c) Staggered Vertical Combs (SVC); d) Angular Vertical Combs (AVC). Adapted from [11].....3

Figure 3 - Variation of damping ratio with natural frequency of a system. Adapted from [21]. 9

Figure 4 - Overview of MEMS+®. Adapted from [14].....10

Figure 5 - SOIMUMPs microfabrication steps.....11

Figure 6 - 3D model of the direct drive micro-mirror 13

Figure 7 - a) MEMS+® direct drive micro-mirror; b) CoventorWare® direct drive micro-mirror. Adapted from [4]. 13

Figure 8 - 3D model of the direct drive micro-mirror: mechanical connectors view.....14

Figure 9 - Q Factor extraction. Experimental frequency response adapted from [4] 15

Figure 10 - Difference between mechanical and optical angle.....15

Figure 11 - Direct drive micro-mirror: Torsional Mode.....17

Figure 12 - Direct drive micro-mirror: Capacitance variation with angle 18

Figure 13 - Direct drive micro-mirror: Change on Capacitance and Angle with Voltage 19

Figure 14 – $dC/d\theta$ vs Angle, comparison between CoventorWare® and MEMS+®.....19

Figure 15 - Direct drive micro-mirror: Frequency response at 3 different timespans.....20

Figure 16 - Direct drive micro-mirror: Frequency response at 3 different numerical configurations 21

Figure 17 - 3D model of the indirect drive micro-mirror 23

Figure 18 - 3D model of the indirect drive micro-mirror: mechanical connectors view.....24

Figure 19 - Different meshes on indirect drive micro-mirror. a) Mesh on frame; b) Mesh on Mirror; c) Mesh on comb-finger. 25
Figure 20 – Torsional modes of the Indirect drive micro-mirror: a) Out-of-phase mode; b) In-phase mode 29
Figure 21 - Frequency response at down sweep of the indirect drive micro-mirror having 3 different types of comb-drives (A, B and C) 30
Figure 22 - Frequency response of the indirect drive micro-mirror at different voltages 31
Figure 23 - Resonant frequency for different driving voltages 31
Figure 24 - Frequency Response at 3 different anchor´s arm lengths of the indirect drive micro-mirror 32
Figure 25 - Frequency Response showing the behaviour of the mirror and the frame on indirect drive micro-mirror 33
Figure 26 - Frequency Response of the indirect drive micro-mirror at both down and up sweep 33
Figure 27 - Frequency response at down sweep of the indirect drive micro-mirror and phase 34
Figure 28 - Frequency Response of the indirect drive micro-mirror: Comparison between MATLAB® and Simulink® 35
Figure 29 - Simulink® schematic for transient simulation on indirect drive micro-mirror 35
Figure 30 - Schematic of SOIMUMPs microfabrication steps. Adapted from [23] 43
Figure 31 - MEMS+ Innovator tab. a) Tabs; b) Components; c) Outputs; d) Component properties: Deposits; e) Component properties: FEM model; f) Variables; g) Mechanical connectors; h) Electrical connectors 44

Figure 32 - MEMS+ Simulator Tab. a) Analysis; b) Exposed Electrical Connectors; c) Exposed Mechanical Connectors; d) Exposed Connector Properties; e) DC/Force sweep properties.....45

List of Tables

Table 1 - Modal Analysis on direct drive micro-mirror: results from 3 different simulators..16

Table 2 - Defining damping in the desired parts on the comb-finger.....26

Table 3 - Q Factor variation by applying different values of Rayleigh damping beta, according to equation (13).....28

Table 4 - Modal Analysis on indirect drive micro-mirror.....28

Table 5 - Dimensions of the comb-drives: A, B and C.....29

Table 6 – Damping Coefficients, Q Factors and Rayleigh damping alpha of the indirect drive micro-mirror.....37

Table 7 - SOIMUMPs material properties.....46

Motivation

Many decades have passed since the discovery of MEMS devices. Nowadays, they are being used in our every-day life, in our car, our smartphone, TV, video games. The list is certainly much bigger and they can be as diverse as accelerometers, gyroscopes, microphones, micro-mirrors and a bunch of many other devices. They are everywhere, and still, invisible to the user´s eyes, since they are usually encapsulated and hidden inside bigger devices. Beside their invisibility at a macro scale, at a micro and nano scale, they are very complex structures, containing a lot of different materials, and acting in a very sensitive way, that can be amplified until it reaches our senses.

Even with the maturity of fabrication and commercialization, MEMS is still one of the hottest developing areas in science and engineering. Designers are now aiming to achieve complicated objectives while meeting a long list of specifications related to sensitivity, fabrication, system integration, packaging, and reliability. These challenges have created a motivation to seek new solutions and ideas. [1]

Scanning micro-mirrors can meet the high-resolution, low-power consumption, and high-scanning speed requirements in demanding applications, such as pico-projection and medical applications. How effectively the device performs its function will depend to a large degree on the underlying resonant characteristics of the device (e.g., its quality factor, which determines the resonant peak ”sharpness” on a plot of response vs driving frequency). [2], [3]

For the development of these kind of micro-mirrors, several architectures can be implemented, some aiming for direct drive, others aiming to indirect drive. Ones can be implemented in a raster scanning system, others in a Lissajous system. The processes of micro-fabrication are numerous and the types of actuation can vary between electrostatic, piezoelectric, electrothermal, electromagnetic and others. The options in this field are so diverse and rich, that allows engineers to boost their creativity.

Objectives

This project aims to develop a lumped model of two electrostatically actuated resonant micro-mirrors using *MEMS+®*, *CoventorWare®* and *MathWorks®*. Both types have SOIMUMPs from MEMSCAP as target process. The first type is a direct drive micro-mirror, and it's presented in [4]. The main objective in this chapter will be to design the micro-mirror as close as possible to the one in [4], and perform the same simulations presented. The software packages used in it are both *CoventorWare®* and *ANSYS®*, and it's possible to test *MEMS+®* reliability by comparing both results. The second is an indirect drive micro-mirror, which is already designed, using *ANSYS®*, by the Department of Microelectronics & Nanoelectronics of the University of Malta (DMN/UM). The same design has to be developed using *MEMS+®*, and the simulations performed on the direct drive mirror will then be implemented in this one. The latter should follow certain constraints, such as: 25 kHz resonant frequency at the torsional mode, 12 degrees of scanning angle, 200 V of driving voltage and an amplification factor of 5.

CHAPTER 1: INTRODUCTION

1. Resonant Micro-mirrors

1.1. Laser Scanning for Pico-Projection

Reflective projection displays are a growing field in micro-electromechanical-system (MEMS) devices. Reflective miniaturized laser projectors, also called pico-projectors, are expected to become more and more widespread, as a consequence of the increasing interest on exchanging and sharing directly from mobile devices (smartphones, tablets or digital cameras) multimedia contents, such as images, videos or presentations. The small screen of the latter devices, could be overcome by multimedia projection on several kinds of surfaces. [5]

The three currently competitive technologies for miniaturized projectors are MEMS laser scanning, digital micro-mirror devices (DMD), and liquid crystal on silicon (LCoS) displays. Regarding laser scanning, the main advantages are the high colour gamut, scalability of resolution within the same footprint, and an always-in-focus image. MEMS scanners can be classified according to the following three categories: operation principle (reflective mirror, refractive lens, and diffractive grating), actuation principle (mainly electrostatic, electromagnetic, piezoelectric, and electrothermal), and fabrication technology (e.g. bulk micromachining, surface micromachining, and hybrid fabrication methodologies). [6]

The performance of a display scanner, is based on working frequency, scan angle, mirror size, mirror flatness (dynamic and static), good mode separation (resonant scanners), and linearity. The two latter points are relevant to image quality, while the others directly determine limits for resolution and image size. [6]

For pico-projection, one of the most common system architecture is raster scanning, where two single micro-mirrors are paired, one operating at low frequency, linear vertical scan (quasistatic) and another operating at high frequency, resonant horizontal scan. [6], [7]

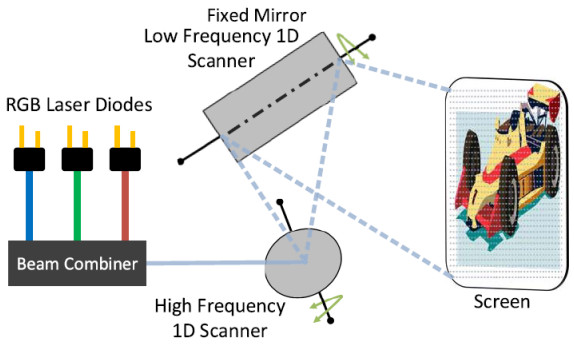

Figure 1 – Raster scanning architecture where each mirror is responsible for each axis. Adapted from [6].

1.2. Actuation Principle: Electrostatic

Many actuators are considered for scanning micro-mirrors, for example, electrostatic actuators, piezoelectric actuators, electrothermal actuators, electromagnetic actuators, pneumatic actuators, and shape memory alloy. [8]

When comparing scanners for commercial use, the most critical aspects to consider are: enabled resolution, fabrication simplicity, power efficiency, voltage requirement, robustness, compactness, and long-term stability. Electrostatic actuation provides long-term stability, size advantages, and fabrication schemes which are easier to render CMOS compatible. On the other hand, it requires high voltages to operate, and is sensitive to inexactness in microfabrication due to the pull-in phenomenon. Piezoelectric actuators have issues of charge leakage and hysteresis of materials. For electrothermal and electromagnetic actuators, power consumption is a problem, also electromagnetic actuators require external magnets that can be large in size and can create electromagnetic interference. [6], [8]

There are two main types of electrodes that are often used for electrostatic actuation: parallel plates and interdigitated combs. The first ones generate sensing and actuation across planer electrode facing each other, and the second ones take advantage of capacitance generated from sidewalls of electrodes. Such capacitors provide alternative fabrication and operation modes compared with parallel-plate capacitors. Generally, they consist of one stationary and one movable set of interdigitated comb fingers that are operated by applying an electrostatic field between them. [9], [10]

In case of parallel plates, capacitance is given by:

$$C = \frac{\varepsilon_0 \varepsilon A_0}{d} \tag{1}$$

Where ε_0 is the absolute permittivity, ε is the dielectric constant of the medium, A_0 is the common area between plates and d is the distance between the plates. In case of comb-drives, the capacitance is given by:

$$C = \frac{N \varepsilon_0 \varepsilon l_0 t}{g} \tag{2}$$

Where N is the number of comb-fingers, l_0 is the length of the fingers, t the vertical thickness and g the gap between them.

In many electrostatic actuators that are fabricated by current micromachining processes, the nominal gap between the electrodes is not negligible relative to the lateral dimensions of the deformable capacitor. Therefore, fringing fields are considerable and must be accounted

for when modelling the electrostatic forces. The capacitance between a pair of electrode fingers is contributed by vertical surfaces of the finger in the overlapped region, as well as by fringe capacitance fields. Capacitances derived from multiple finger pairs are connected in parallel. Hence, the total capacitance is a summation of capacitance contributed by neighbouring fingers. Fringe capacitance is given by Palmer formula: [9]

$$C_f = \varepsilon \frac{w l_0}{g}\left(1 + \frac{g}{\pi w}\left(1 + \ln\left(\frac{2\pi w}{g}\right)\right)\right) \times \left(1 + \frac{g}{\pi l_0}\left(1 + \ln\left(\frac{2\pi l_0}{g}\right)\right)\right) \quad (3)$$

Where w is the width of the finger. The overall capacitance is given by:

$$C = \frac{N\varepsilon_0 \varepsilon l_0 t}{g} + C_f \quad (4)$$

There are currently four categories of comb-drive designs: lateral combs, rotary combs, staggered vertical combs (SVC), and angular vertical combs (AVC). [11] These are expressed in the Figure 2 below:

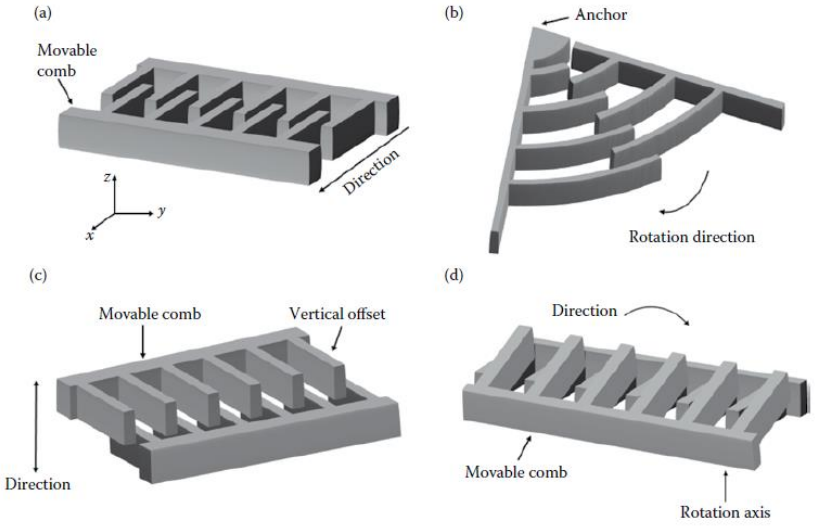

Figure 2 – Comb-drive designs: a) Lateral Combs; b) Rotary Combs; c) Staggered Vertical Combs (SVC); d) Angular Vertical Combs (AVC). Adapted from [11].

In the case of AVC illustrated in Figure 2d), the movable combs are often fabricated in the same layer as the fixed fingers and then tilted upward by various post-fabrication methods such as plastic deformation, residual stress and manual assembly. In the lateral and vertical comb actuation setups, the force is independent of the displacement, unlike that of the parallel plate actuator setup. In addition, the force is inversely proportional to the gap distance making the force generated much smaller than that of the parallel plate actuator. This can be enhanced by adding more fingers or applying a higher voltage. [11]

The amount of torque produced by the comb actuators as a function of the tilt angle is given by:

$$M(\theta) = N\frac{1}{2}\frac{dC}{d\theta}V(t)^2 \tag{5}$$

Where N is the number of comb-fingers of the mirror.

$M(\theta)$ is proportional to the rate of change of the energy stored in the actuator combs with respect to θ. Change in the stored energy is proportional to the change in the total capacitance of the comb actuators, which is proportional to the overlap area of comb-fingers. Overlap area between the finger plates is a piecewise continuous function with three different regions. When fringing fields are ignored, the rate of change of total capacitance with tilt angle can be found by expressing the overlap area of the comb fingers as a function of θ. The resultant function is piecewise and can be expressed as: [12]

Case I (when $\theta < \frac{t}{\frac{D}{2}+l_0}$)

$$\frac{dC}{d\theta} = -\frac{3\varepsilon}{2g}\left(\frac{D}{2}+l_0\right)^2\theta^2 + \frac{2\varepsilon}{g}t\left(\frac{D}{2}+l_0\right)\theta + \frac{\varepsilon}{g}\left(\frac{{x_0}^2}{2} - \left(\frac{D}{2}+l_0\right)x_0 - \frac{t^2}{2}\right) - \varepsilon\frac{\left(\frac{D}{2}+l_0\right)}{(l_0-x_0)}w \tag{6a}$$

Case II (when $\frac{t}{\frac{D}{2}+l_0} < \theta < \frac{t}{\frac{D}{2}+l_0-x_0}$)

$$\frac{dC}{d\theta} = \frac{\varepsilon}{2g}x_0\left(\frac{D}{2}+l_0-x_0\right) - \frac{\varepsilon t^2}{2g\theta} \tag{6b}$$

Case III (when $\theta > \frac{t}{\frac{D}{2}+l_0-x_0}$)

$$\frac{dC}{d\theta} = 0 \tag{6c}$$

Where D is the mirror width and x_0 the initial overlap of the fingers.

When $V(t)$ is a periodic function, such as a sinusoid, the torque turns out to be a function of both time and angular displacement. Therefore, (7) becomes a nonlinear differential equation with time-varying coefficients. This suggests that the resultant system is a parametric oscillator and will exhibit parametric resonances, and subharmonic oscillations. [12]

1.3. Design Techniques

There are two major factors in the development of micro-mirrors. The first is the integration of mechanical and actuating components and the second is the suitability of fabrication process. The first is ruled by the laws in mechanical, electrostatic, and fluidic fields, and is therefore a fundamental factor, while the latter is related to the development of micro-machining technology. The design techniques for torsion micro-mirrors should take the combination of these factors into account, for that, the following steps must be followed: 1- Identification of design specifications; 2 - Concept generation and fabrication consideration; 3 - Preliminary design; 4 - Numerical simulation and design optimization, such as finite element models (FEM) which has been widely used as valuable tool to accurately predict the field behaviour of electrostatic torsion micro-mirrors, such as torsion stiffness, resonant frequency, and electrostatic torque; 5 - Implementation of fabrication process; 6 - Experimental evaluation.

For the steps 2, 3 and 4 a broad range of modelling and simulation tools is available, such as *ANSYS*®, *CoventorWare*® and *MEMS+*® from *Coventor*®. The latter can simulate the entire MEMS device, including gas damping effects and control circuitry. With *MEMS+*®, designers can run time-dependent and closed-loop simulations that reveal dynamic behaviour that here-to-fore could only be observed and quantified through time-consuming measurements on prototypes (more information about this software in 3). [13], [14]

Regarding the mechanical field, main design specifications for an electrostatic torsion micro-mirror include mirror size, resonant frequency, operation voltage, and rotation angle. Thus, the primary design parameters in mechanical field comprise: The dimensions of the torsion beams; the dimensions of the mirror plate and the gimbal, if it has one; the metal layer used for high reflectivity, which might induce a slight curvature in the mirror by residual stress. [4], [13]

1.4. Direct and Indirect Drive

In a scanner with direct drive the torque is imparted directly from the actuation mechanism to the frame containing the mirror. The indirect drive makes use of a favourable resonance mode to amplify a small motion in a larger mass to a considerably larger motion in the smaller mirror. [6]

The structure of an indirect drive micro-mirror, usually has the comb-fingers placed on an outer frame, and the motion is transferred to the inner mirror frame with a mechanical gain, the difference between the highest angle reached by both the inner and the outer frame, is denoted as amplification factor (*A*). The design intent is to improve actuator efficiency by removing the high-drag fingers from the high-velocity scanning mirror. Placing them on the lower velocity drive frame reduces their contribution to the damping torque. Furthermore, placement on the drive frame allows an increase of the number of fingers and their capacity to impart torque.

Regarding the indirect drive micro-mirrors, there are two scanner operation modes, one being out-of-phase and the other one being in-phase with respect to the two frames. At lower vibration frequency, the inner and outer frames move in phase, whereas at higher vibration frequency, the frames move out of phase. [2]

1.1. Dynamic behaviour

Comb-actuated micro-mirror devices exhibit a hysterical behaviour and generate subharmonic oscillations. This usually occurs for nonlinear parametric systems. It is known that the general equation of motion for a scanning micro-mirror can be written as follows: [12]

$$I_m \frac{d^2\theta}{dt^2} + c\frac{d\theta}{dt} + K_s\theta = M(\theta) \tag{7}$$

Where θ is the tilt angle, I_m the mass moment of inertia, c is the damping constant, K_s is the torsional stiffness and $M(\theta)$ the torque function.

The electrostatic torque, generated by the vertical comb drive structure is dependent on the non-linear variation of the capacitance, C with scan angle as in: [12], [15]

$$M(\theta) = N\frac{1}{2}\frac{dC}{d\theta}V(t)^2 \tag{8}$$

Where N is the number of fingers of the mirror.

The damping c and the electrostatic forcing torque $M(\theta)$ are highly non-linear. The main damping sources are the fluid pressure drag and viscous shear forces acting on the scanning mirror under atmospheric air conditions. [15]

The non-linearities give rise to a bistable system response exhibiting the phenomenon of parametric resonance. A periodic excitation at frequencies $f = 2f_0/n$ for $n = 1, 2, 3$ ... is capable of exciting the resonance frequency, f_0 [15], [16]. For the out of plane torsion mode, the resonant frequency is obtained according to: [17]

$$f_0 = \frac{1}{2\pi}\sqrt{\frac{K_s}{I_m}} \tag{9}$$

At the resonant frequency, f_0, the peak scan angle amplitude or the maximum mechanical scan angle, θ_{MMSA} is achieved by sweeping the drive signal frequency downwards from a higher frequency. In order to achieve high mirror scan angles, the electrostatic energy has to overcome the energy loss due to air damping. Energy dissipation due to air damping in resonant micro-mirrors is derived from two main sources: Comb-drive structures and mirror plate oscillations. The viscous fluid motion around the comb-drive structure gives rise to a velocity gradient normal to the finger surface, this results in a shear force, on the moving finger proportional to the air viscosity. The mass transport of air due to large scan angle oscillations of the mirror plate induces pressure drag. The resultant force is proportional to the area of the mirror plate normal to the flow direction. At the bottom surface of the cavity may rise squeeze film damping. However, squeeze film damping effects can be neglected for micro-mirrors having a cavity depth to mirror diameter ratio greater than 0.1. [15] Structural damping is also present, it is primarily caused by crystallographic defects like dislocations, twins, and grain boundaries that affect the propagation of stress waves through the material. Structural damping depends on both the material and the manufacturing technique. However it is usually neglected on MEMS, once it has more significance on smaller devices. [18]

Typically, damping in MEMS is reported in terms of the quality factor Q, the ratio of energy loss per cycle of free oscillations to the total system energy. [19] For the torsional motion of the micro-mirror, the quality factor can be approximated as: [17]

$$Q = \frac{1}{c}\sqrt{K_s I_m} \tag{10}$$

The total quality factor Q can be expressed in terms of the individual quality factors as:

$$\frac{1}{Q} = \frac{1}{Q_1} + \frac{1}{Q_2} + \cdots = \sum_j \frac{1}{Q_j} \tag{11}$$

It is clear from (11) that the total quality factor is limited by the smallest component. Q cannot exceed any of its components. Hence, damping in MEMS, a vital step is to determine the dominant dissipation mechanism since it controls the overall damping. [20]

Quality or damping factors, whether computed or experimentally measured, may be used in time or frequency domain simulations by converting them to Rayleigh damping coefficients α and β, or modal damping factor ζ. [18] The most effective way to treat damping within modal analysis framework is to treat the damping value as an equivalent Rayleigh damping in form of: [21]

$$[c] = \alpha[M] + \beta[K_s] \tag{12}$$

In which $[c]$ = damping matrix of the physical system; $[M]$ = mass matrix of the physical system; $[K_s]$ = stiffness matrix of the system; α and β are pre-defined constants. These are also called as mass proportional and stiffness proportional respectively. [22]

The major advantage gained in converting the damping matrix into an equivalent Rayleigh damping lies in the fact that using orthogonal transformation a structure having n degrees of freedom can be reduced to n-number of uncoupled equations. [21]

The orthogonal transformation of the damping matrix reduces the matrix $[c]$ to the form (valid at the resonant frequency ω_0): [21], [18]

$$\zeta = \frac{c}{c_{critical}} = \frac{1}{2Q} = \frac{\alpha}{2\omega_0} + \frac{\beta\omega_0}{2} \tag{13}$$

In which $c_{critical} = 2\sqrt{K_s I_m}$. From (13) it can be observed that the damping ratio is proportional to the natural frequencies of the system. A typical plot of the equation $\frac{\alpha}{2\omega_0} + \frac{\beta\omega_0}{2}$ is shown below: [21]

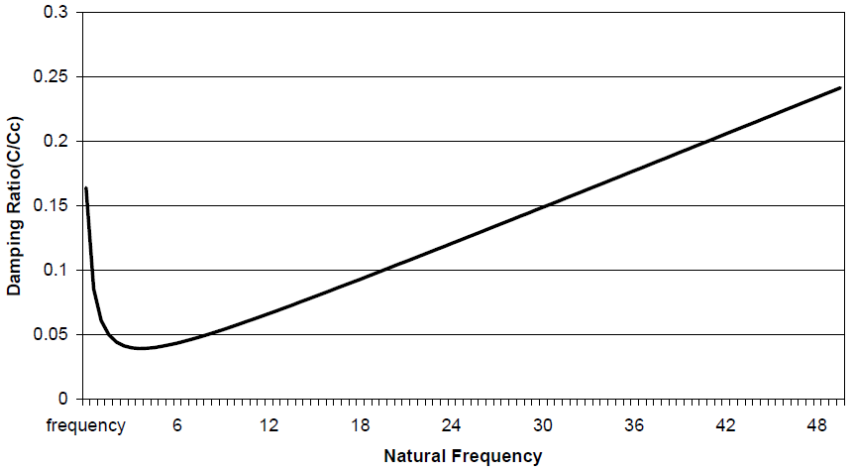

Figure 3 - Variation of damping ratio with natural frequency of a system. Adapted from [21].

In the Figure 3 above, at the first few modes there is a significant mass participation. It can be concluded that when f_0 is small, $\frac{\alpha}{2\omega_0}$ dominates at the initial stage, and as f_0 increases the value $\frac{\alpha}{2\omega_0}$ diminishes and approaches zero and the term $\frac{\beta\omega_0}{2}$ starts dominating the equation and there is an increase on stiffness participation. [21]

That is why, when converting a single damping or quality factor to Rayleigh coefficients, either α or β may be specified, with the other set to zero, unless operation is near to the transition point. In the frequency domain, Rayleigh coefficients apply over the entire range of driving frequencies, so when computed from a quality factor or damping factor, either of which is associated with a particular resonance, the Rayleigh approach is most accurate around that resonance. [18]

2. Target Process: SOIMUMPs

The Multi-User MEMS Processes (*MUMPs*®), is a commercial program that provides cost-effective, proof-of-concept MEMS fabrication to industry, universities, and government worldwide. Three standard processes as part of the *MUMPs*® program, are offered by MEMSCAP: PolyMUMPs, a three-layer polysilicon surface micromachining process; MetalMUMPs, an electroplated nickel process; and SOIMUMPs, a silicon-on-insulator micromachining process. The SOIMUMPs process is a 4-mask level SOI patterning and etching process. [23] The process steps are described in A.

3. *MEMS+®*

MEMS+® is a software platform for engineers who design MEMS devices and it integration with CMOS circuits and packaging. It is appropriate for designing and optimizing MEMS-based components, such as: motion sensors, microphones, micro-mirrors, micro-switches, timing devices and energy harvesters. [24]

MEMS+® users assemble advanced finite elements, or fundamental MEMS-specific building blocks, into a completed design. The obtained designs, provide simulation results up to 100 times faster than conventional finite element analysis tools. This improvement in simulation time makes it feasible to analyse complex multiphysics behaviour and improve the performance and reliability of product designs. *MEMS+®* designs can be directly included in *MathWorks®* and *Cadence®*. [24]

The software is based on an extensive library of MEMS components. Each of them has a 3D view and an underlying model that captures mechanical, electrical and/or gas damping physical behaviour. By assembling the models from its component library and defining electrical, mechanical, input and output ports in MEMS+ Innovator, MEMS+ models are ready for simulation. The integration with *MathWorks®* and *Cadence®* is able to automatically and instantaneously convert a given Innovator schematic into a symbol and corresponding model without requiring time-consuming FEM analysis. [25]

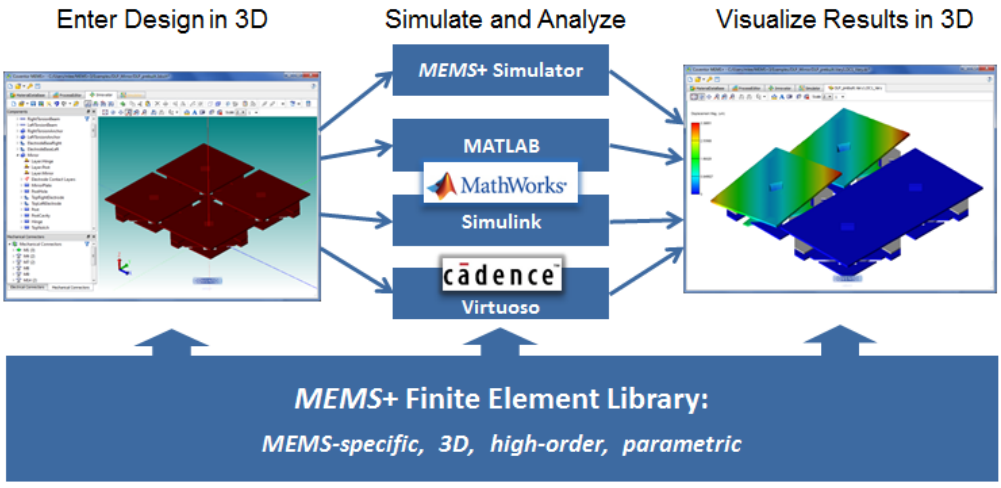

Figure 4 - Overview of MEMS+®. Adapted from [14]

CHAPTER 2: DIRECT DRIVE MICROMIRROR

This chapter aims to design and simulate the direct drive micro-mirror presented on [4], using both *MEMS+*® and *MATLAB*®. The first will be use to design, perform modal and DC analysis. *MATLAB*® allows to import the design previously developed on *MEMS+*® and perform transient analysis on it.

1. Process and Materials

Before starting the design, the process and materials had to be specified. When opening *MEMS+*®, five tabs are shown, the first one it's called *MaterialDatabase*. A file having SOIMUMPs materials was imported to *MEMS+*® and it had the properties of each material of the target process. Some of these material properties had to be changed according to [4], such as silicon's density, Young modulus and residual stress. All the materials properties can be seen in Table 7 on B. Note that it is very important that the residual stress is defined, once it will contribute to create a curvature in the mirror after the metal deposition. This curvature enhances the torque because it creates a vertical offset, unfortunately it also decreases the maximum angle achieved by the mirror and it leads to beam convergence/divergence. [4]

On the *ProcessEditor* tab, SOIMUMPs fabrication steps are defined according to [23]. The microfabrication steps are expressed in the Figure 5 below.

Step	Material	Colour	Thickness (µm)	Mask Name	Mask Offset	Sidewall Angle	Wafer Side
Substrate	**Silicon**		**400**				
DRIE				Trench	0	3.6	Back
ThermalOxidation	Thermal Oxide		1				
DRIE2				Trench	40	0	Front
DRIE3				SOI	0	0	Front
GrowCrystalSi	Silicon on Insulator (SOI)		25				
DRIE3				SOI	0	0	Front
DRIE3				SOI Hole	0	0	Front
EBeam	PAD Metal		0.52				
Lift Off				PadMetal	0	3.6	Front
MetalDep1	Blancket Metal		0.65				

Figure 5 - SOIMUMPs microfabrication steps

2. Design

The *Innovator* tab, allows to perform the design of the micro-mirror from [4]. In order to design it, the dimensions expressed in [4], were defined as variables (Figure 31 in B) in *MEMS+®.* Also, values as temperature, pressure and damping were defined. The last one, was extracted using a method explained ahead in 3,

By creating parameters, it is possible to optimize the design without redesigning new blocks with new dimensions, thus reducing the optimisation time. The blocks available in the software are both rigid and flexible, the latter ones were used since it would not be possible to observe the curvature created by residual stress on the rigid structures. Also, the flexible blocks, allow for more precise simulations since they have more degrees of freedom. The blocks used for this micro-mirror were mostly rectangular plates, nevertheless serpentines and comb structures were also used.

In plate´s properties, it is possible to specify the origin, dimensions and other parameters, using the variables defined previously. The layer which the plate corresponds, must also be defined, and for most of the blocks, the one used was the *GrowCrystalSi* (Figure 5). Nevertheless, a centre plate was defined with two layers, both *GrowCrystalSi*, and *MetalDep1*. The latter layer corresponds to an alloy of 50 nm Cr + 600 nm Au, and it is used to improve the reflectivity. This block was afterwards defined as the *mirror,* since it will be the zone where the light will focus. Also, the overlap of these two layers, creates a mechanical stress and induces a curvature in the mirror (Figure 7).

Still in the properties window, it is possible to define the finite element in the block, as *brick element* or *shell element*. The *shell element* was used, since the *brick element* can't be applied in blocks defined with two layers. [26] These elements allow to specify the number of nodes which corresponds to the number of degrees of freedom, and in order to maximize the flexibility of the device, the maximum number of nodes (six) were taken in both axis, in all the components. Note, that by choosing more nodes, more computational time is required.

Having all the variables defined, and all blocks fully parameterized and displaced at *Innovator* tab, it was now possible to observe the 3-D model virtual view of the device in the Figure 6 below:

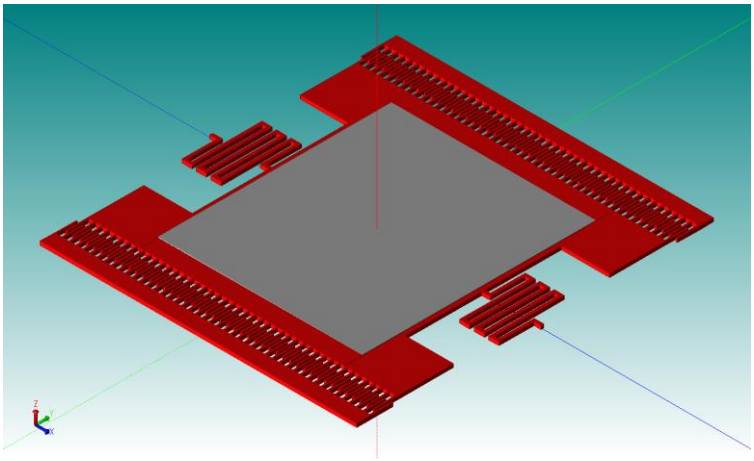

Figure 6 - 3D model of the direct drive micro-mirror

However, the blocks still needed to be joined, and for that, the nodes were used as mechanical connectors. There's a tool that allows for automatic link of the connectors (*Apply Wizard Actions*), unfortunately it showed not to do a proper link for designs with many nodes. Therefore, the connectors were linked manually (Figure 8). Different attempts were tried in order to optimize the specifications expressed in [4], such as frequency of operation (941 Hz) and Z displacement (from -4.2 to 5.9 µm). These optimization was carried out by performing modal and DC analysis on *Simulator* tab, after each modification of the connectors on *Innovator*.

The final step on the *Innovator* tab, was to expose electrical connectors, variables and outputs, such as capacitance. Exposing, allows these parameters to be used on *Simulator* tab, or in *MathWorks® and Cadence®*. Regarding the electrical connectors, only the stators were exposed, the rotors were grounded to create a voltage difference.

The results expressed in Figure 7, show that the design achieved by *MEMS+®* is alike the one from [4]. However slight changes were performed, since there was a lack of information in [4], about the dimensions of certain parts of the micro-mirror.

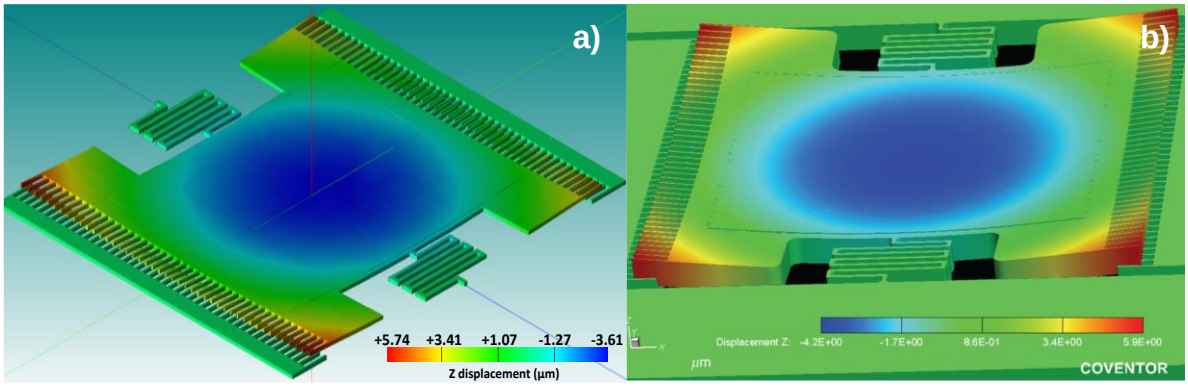

Figure 7 - a) MEMS+® direct drive micro-mirror; b) CoventorWare® direct drive micro-mirror. Adapted from [4].

In Figure 7 above, it is possible to see a small change of the z displacement created by the curvature. The micro-mirror from a) shows a z displacement from -3.61 to 5.74 µm, and b) from -4.2 to 5.9 µm. The obtained offset in a) and b) is 9.35 and 10.1 µm, respectively.

The combination of mechanical connectors, which led to better results is represented in the Figure 8 below:

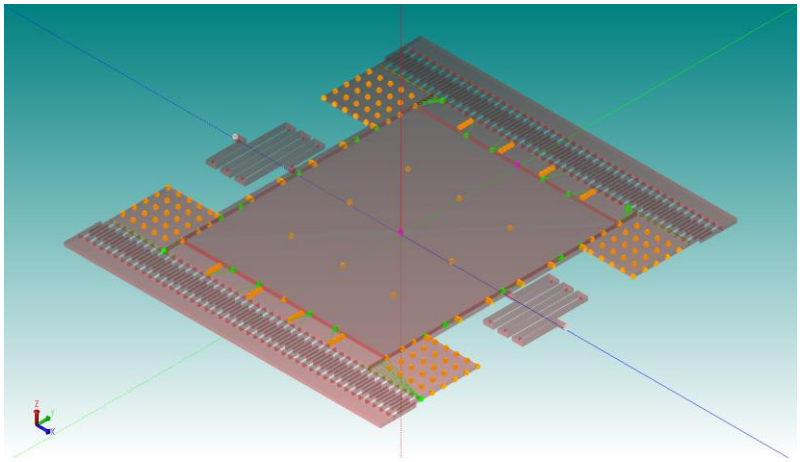

Figure 8 - 3D model of the direct drive micro-mirror: mechanical connectors view

In the Figure 8 above, the green dots are the linked connectors and the yellow ones are the free. Having more free degrees of freedom, leads to more flexibility of the structure, and less computational cost. However, if some mechanical connectors aren't linked, problems might appear in the structure, which can lead to different modes and behaviours in the modal analysis. The same happens with too much linked connectors, so it is important to find an equilibrium.

3. Extracting Quality Factor and Rayleigh damping

In order to perform transient simulations, the Rayleigh damping alpha has to be implemented on the parameters of *MEMS+®*.

MEMS+® does not own a partition for damping extraction, hence Q Factor can't be obtained by this simulator. Two methods of Q Factor's extraction were implemented on the micro-mirrors. For the direct drive micro-mirror, a method using a HPB formula from [28], and for the indirect drive micro-mirror another using *CoventorWare®*.

3.1. Q Factor's extraction using HPB formula

There´s no value of Q Factor in [4] so then, a method performed by [28], was implement to extract it from the experimental frequency response of the device. Figure 9 below, shows the method of extraction.

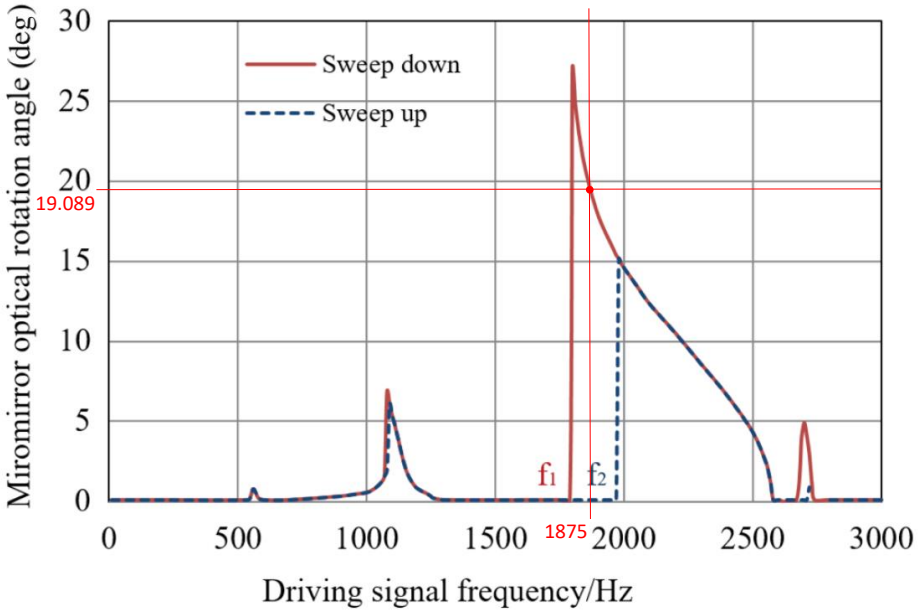

Figure 9 - Q Factor extraction. Experimental frequency response adapted from [4]

In the Figure 9 above, note that the angle represented is the optical angle enhanced by lens. According to [4], the lens amplify the angle by 2.25, and the optical angle is four times de mechanical angle [29], which is 3°, at the resonant peak. The figure below shows the difference between mechanical and optical angle.

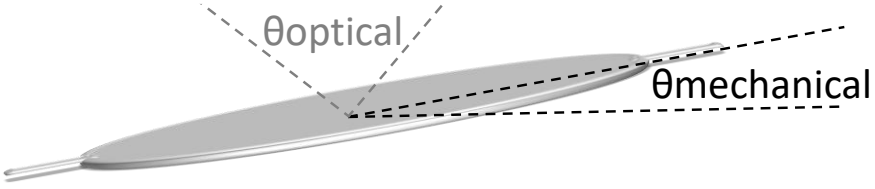

Figure 10 - Difference between mechanical and optical angle

Also note, that the represented frequency is the driving one, which corresponds to double the resonant frequency.

To derive the quality factor from Figure 9, the half-power bandwidth (HPB) formula was used. Let f_0 denote the driving frequency (1800 Hz), and f_1 (1800 Hz) and f_3 (1875 Hz) denote the half power frequencies, where the amplitude of oscillation is $\frac{1}{\sqrt{2}}$ times the driving amplitude (note that the values represented in red are merely approximations). This method of extraction, is usually implemented on linear behaviours, however a plausible value was achieved. The Q Factor was extracted according to: [28]

$$Q = \frac{f_0}{f_3 - f_1} = \frac{1800}{1875 - 1800} = 24 \tag{14}$$

To obtain the damping coefficient from Q, the equation (14) was implemented, β was set to zero and the resonant frequency used was 941 Hz from [4]. The obtained value of alpha is: 246.35.

4. Simulation and results

4.1. Modal Analysis

On the *Simulation* tab (Figure 32 in B) in *MEMS+®* it is possible to set a modal analysis. In the latter, the number of modes can be specified. Since only the first ones are important for this micro-mirror, six modes were specified. By running the modal, another tab appears, showing a 3D behaviour of the mirror at different modes.

4.1.1. Results of the Modal Analysis

The results of the modal analysis, aren't too far from [4], where the modal analysis was carried out using *ANSYS®*. A comparison with *CoventorWare®* was also possible, since the same micro-mirror from [4] was designed and subjected to the same analysis by DMN/UM. In Table 1 below, it´s shown the resonant frequency at six different modes of operation, for the three simulators used.

Table 1 - Modal Analysis on direct drive micro-mirror: results from 3 different simulators

Simulators	1st mode (Torsional)	2nd mode	3rd mode	4th mode	5th mode	6th mode
MEMS+®	940 Hz	2827 Hz	3411 Hz	5093 Hz	5487 Hz	8287 Hz
ANSYS® [4]	941 Hz	2916 Hz	3149 Hz	5111 Hz	5218 Hz	6060 Hz
CoventorWare® (UM)	921 Hz	2688 Hz	2933 Hz	4788 Hz	4989 Hz	5917 Hz

From Table 1, it is possible to see that *MEMS+*® first frequency mode it´s very close to the *ANSYS*® one (from [4]). Overall, the three different simulators show similar frequencies for each mode. Also, the modes are considerably displaced from each other, which assures better performance of the device. The torsional mode (Figure 11), corresponds to the tilt around x axis, and it's the mode at which the micro-mirror must operate.

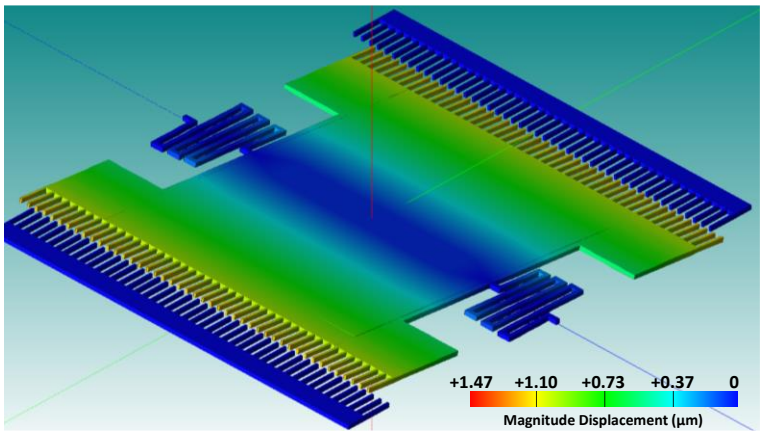

Figure 11 - Direct drive micro-mirror: Torsional Mode

4.2. Force and DC Sweep Analysis

On the *Simulation* tab (Figure 32 in B), a *DC sweep* analysis was specified, however this command can act as a force sweep as well, by choosing the *sweep source*. At the top of the micro-mirror block, a mechanical connector is exposed on the *Innovator* tab. This connector was chosen, because it allows the mirror to bend with a smaller force. Back on *Simulation* tab, a value of 200 µN is applied in the z direction of the exposed connector. Regarding the *sweep source*, it can now be set with the name of the mechanical connector and it respective z direction.

After specifying a linear increment from -800 µN to 800 µN, the analysis was ran, and the results were expressed on the new tab. Variables such as capacitance and angle, were plotted against force, and exported.

Another *DC sweep* analysis was performed, a 100 V voltage was applied on the exposed electrical connector (*StatorTop*) and the latter one was chose as *sweep source.* This voltage was implemented because it is the same as used in [4]. A linear increment from 0 to 500 V was specified and the analysis was ran. The same variables were exported.

4.2.1. Results of the Force Sweep Analysis

The Figure 12 below, shows the behaviour of the capacitance with the angle, produced by the applied force.

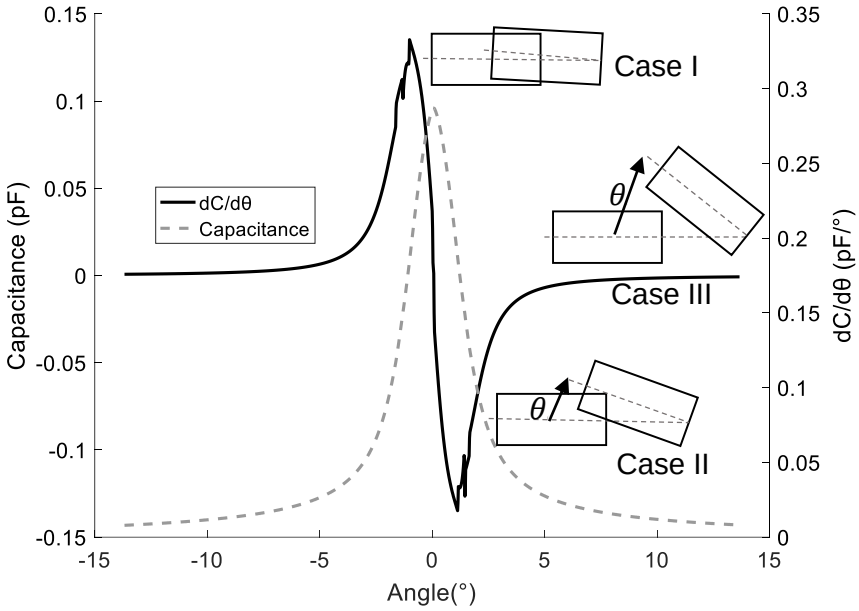

Figure 12 - Direct drive micro-mirror: Capacitance variation with angle

The angle varies linearly with the applied force, however, the capacitance shows a non-linear performance, as it shown on Figure 12. The capacitance is maximum, when the overlap area is bigger (1). Since the mirror shows a small curvature, the capacitance isn't maximum when both rotor and stator are in plane (0°), but immediately after it. At this point (Case I), the capacitance change decays abruptly (6a). At Case II, the overlap area starts to decrease and so the capacitance, nevertheless the capacitance change tends to increase (6b). On Case III, it is possible to notice a linear behaviour which is related to the fact that the fingers start to behave as parallel plates, since there's no overlap area anymore (6c).

4.2.2. Results of the DC sweep analysis

The behaviour of the capacitance and the angle with the applied voltage is shown on Figure 13.

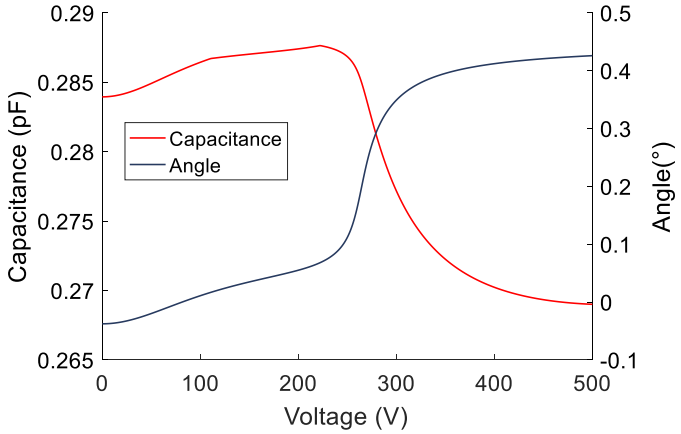

Figure 13 - Direct drive micro-mirror: Change on Capacitance and Angle with Voltage

In the Figure 13 above, it is possible to see that neither capacitance nor angle varies linearly with the applied voltage. The first one increases smoothly until it reaches a point where the electrostatic force is maximum and the pull-in phenomenon occurs. Fortunately, this occurs only after the driving voltage, which is, for this mirror, 100 V. The angle also shows a nonlinear behaviour, and shifts drastically when the capacitance is maximum, and so, the electrostatic force.

4.2.3. Comparing both *MEMS+*® and *CoventorWare*®

The simulations implemented on *MEMS+*®, were also performed on *ConventorWare*® by DMN/UM. Figure 14 shows the capacitance variation with angle derived from simulations carried out by both simulators.

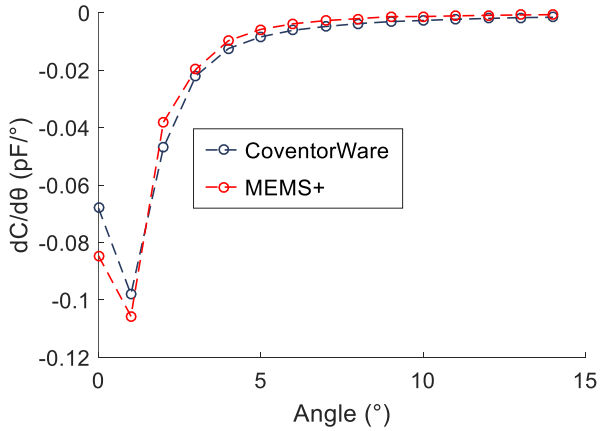

Figure 14 – dC/dθ vs Angle, comparison between CoventorWare® and MEMS+®

In the Figure 14 above, it is possible to see that there is no significant deviation in the capacitance of both simulators. At the beginning, there is a small difference that might be related with the z displacement magnitude of the curvatures in both devices. The maximum capacitance achieved on *CoventorWare®* is larger than on *MEMS+®*, due to a larger overlap area, hence the initial curvature is smaller on *CoventorWare®*.

This difference in magnitude is related with slight changes in the dimensions of the device, especially on the serpentines, comb-drives and the overall size of the mirror.

4.3. Frequency Response

To obtain the frequency response of the micro-mirror, it is necessary to perform transient analysis, the files from the simulation tab in *MEMS+®* were saved. A script to call the latter files was inserted on *MATLAB®* and a function was applied on both stators of the micro-mirror. The full script can be found in C.

4.3.1. Frequency response at different timespans

The *timespan* is the time that the simulation takes to go through a certain range of frequencies. A *chirp* function (explained in C) was used, the frequency changes linearly with time, and so, it is expected that a bigger *timespan* may result in a more defined frequency response, the Figure 15 below, shows the comparison of three frequency responses with three different *timespans.*

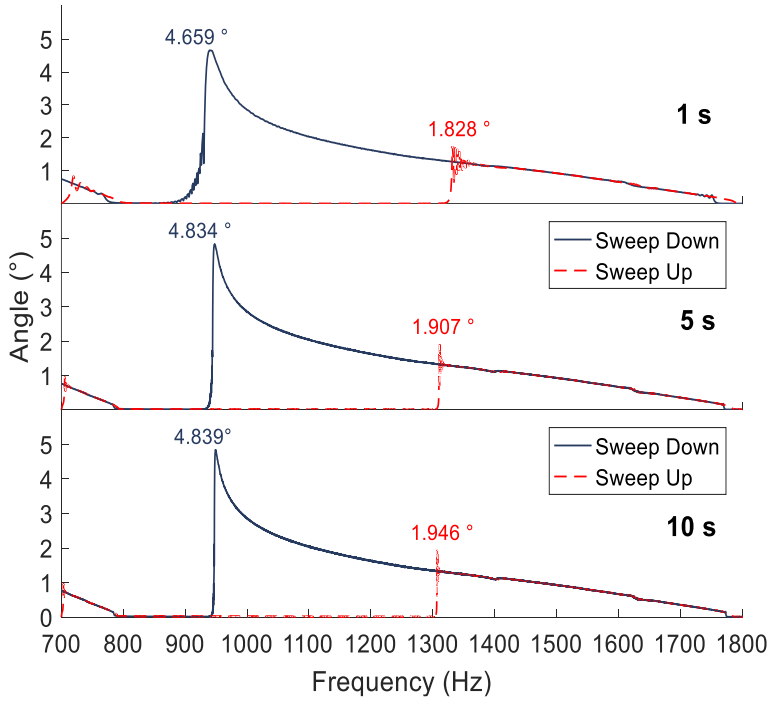

Figure 15 - Direct drive micro-mirror: Frequency response at 3 different timespans

In Figure 15 above, it is possible to observe that the best result matches the biggest *timespan* (10 s), as expected. The angle peaks are higher in this one and both down and up sweep show a very sharp behaviour at the resonant frequency. The frequency at down sweep is the relevant one, since the mirror has to be driven at higher frequencies first, and the values for the three different *timespans* are: 939.1 Hz (1 s), 947.7 Hz (5 s), 949.5 Hz (10 s). The first one, is the one that is closer to the value from [4], 941 Hz, nevertheless doesn't show the best behaviour, and it's only good to use this *timespan* for optimization, since the computational cost is much lower compared to the others. The achieved angle is similar in the three different timespans and it almost matches de mechanical angle from [4].There is no information about the mechanical angle in [4], however from [29], it´s known, that the optical angle (12º in [4]) is four times the mechanical one, so it is possible to assume a value of 3º for the mechanical angle in [4].

4.3.2. Frequency response at different numerical configurations

Different numerical configurations were tested. The configuration A (used in 4.3.1), is a complex one, meaning it has six nodes on each block, and five on the central one called *mirror*. B it's the most complex configuration and differs from the A, only on the central block (*mirror*) which now has six nodes. C is a simpler one, with less nodes on each block. The Figure 16 below shows the frequency response of each configuration at 5 s *timespan*.

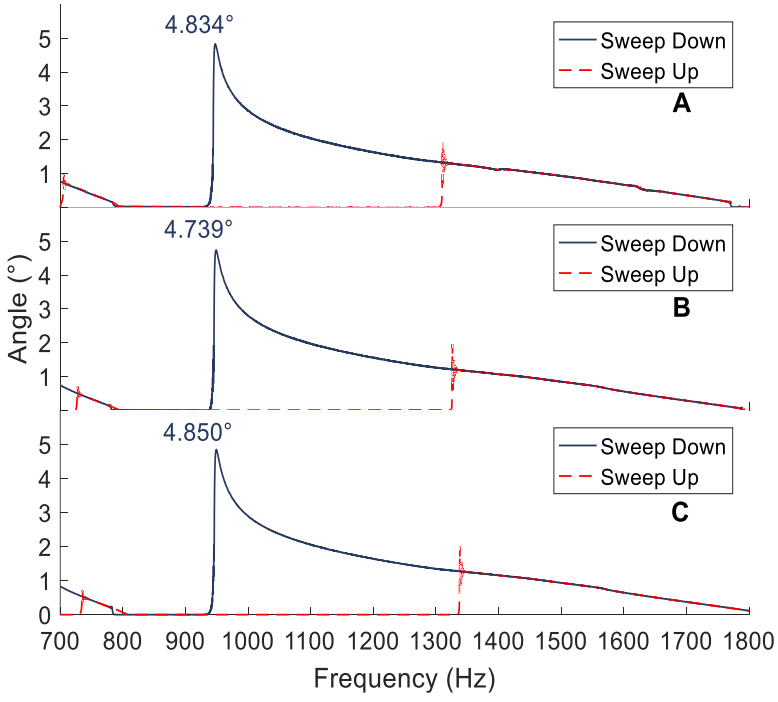

Figure 16 - Direct drive micro-mirror: Frequency response at 3 different numerical configurations

The three different results in Figure 16, have a very similar and sharp behaviour at the resonant frequencies. The main difference seems to be noticed between 700 and 800 Hz, where a second peak appears. This peak it's also shown in Figure 9 around 1100 Hz (driving frequency), and both down and up sweep lines are overlapped, which means, that the configuration A it's a better match for [4], since it's the only one who has more defined overlap between up and down sweep at this peak. With respect to the angle, the biggest one is presented in C as well as the resonant frequency (949.3 Hz). However, a lower value of frequency is demanded, and so, the configuration A is still a better choice. The main advantage of C compared to the other two, is the simulation time, which is slightly lower.

CHAPTER 3: INDIRECT DRIVE MICROMIRROR

1. Design

The design of the indirect drive micro-mirror, was developed before by DMN/UM, using *ANSYS*® as simulator. It was not possible to export a compatible format from this software to *MEMS+*®, however a layout file containing the micro-mirror dimensions was possible to open in the latter. Just like the direct drive micro-mirror, the dimensions were defined as variables, nevertheless they were defined with special attention since optimization would be performed later, hence only certain variables were exposed, the ones that would be subject to modifications.

Flexible components, such as *rectangles*, *arcs*, *fillets* and *pies*, were used to build up the micro-mirror inside the layout limits, and *shell elements* were chosen as finite elements.

This mirror is divided in three main parts: *comb-fingers*, *frame* and *mirror* (containing a gimbal and springs in both sides). This design also contains a reflective layer in the *mirror* part, which will lead to a slight curvature. The 3D model virtual view is shown in Figure 17, below.

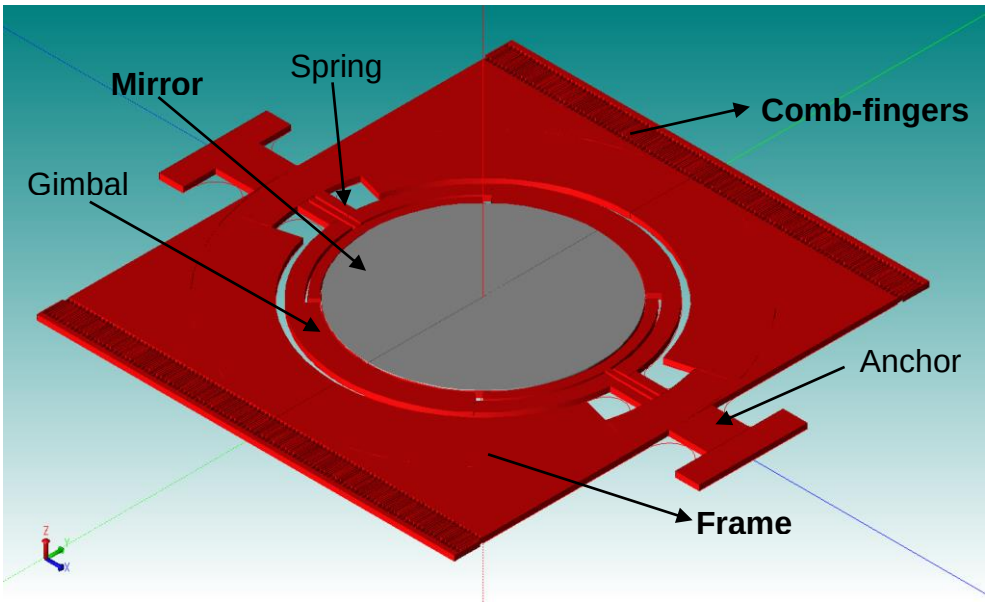

Figure 17 - 3D model of the indirect drive micro-mirror

From Figure 17, it is possible to see that the *frame* is connected to the comb-fingers, however the *mirror* isn´t drive by them. A small motion is amplified in the larger mass (*frame*), when the device is at the resonant mode, and the *frame* amplifies a larger motion in the smaller mass (*mirror*).

Some modifications from the original design had to be implemented, otherwise the file would be too large, and the transient simulations would take a lot of time.

Regarding the mechanical connectors, a lot of combinations were tried. Since this mirror has much more components than the direct drive one, also much more connectors can be implemented. However, it was not suitable to have all the components inputted with high number of nodes, since the computational cost would be too high. Six nodes were used, only in the *mirror* part. All the other components were defined with three or two nodes. The main reason why the *mirror* must be defined with more degrees of freedom, it´s because it is the part of the device which will curve, due to the residual stress created by the reflective layer and will be the part reaching the higher angle. Since flexibility is needed in the *mirror*, most of the connectors were set free (yellow dots) in this part, as it is possible to see in Figure 18 below:

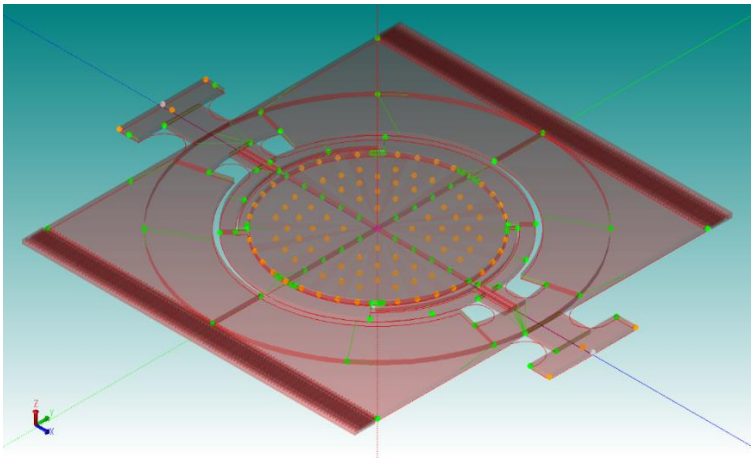

Figure 18 - 3D model of the indirect drive micro-mirror: mechanical connectors view

Having the other parts of the device defined with less nodes, didn´t affect the modal analysis, and the desired resonant frequency at the torsional mode was reached.

2. Extracting Q Factor and Rayleigh damping

2.1. Q Factor's extraction using *CoventorWare*®

The design was exported to *ConventorWare*® from the *Innovator* tab on *MEMS+*®. When opening the imported model in *CoventorWare*®, different layers of the device are shown. The silicon layer was separated in parts, and for that partitions were created in order to separate the device in three main parts: *mirror, frame* and *comb-finger* (Figure 17). Having all the desired partitions, they were selected and meshed. Meshing the model, means to reduce the structure to a group of simpler finite element bricks, and present to the solver to finite element analysis. [30] Three different meshes were performed, one in each desired part of the device

(*mirror, frame and comb-finger*) (Figure 19). These parts were chosen, because the damping effect is different in each one, and the overall Q Factor of the device it is more reliable when combining them according to (11). For example, the *mirror* reaches a bigger angle than the *frame*, due to the amplification created by the latter, so the damping acts differently, as well as on *comb-fingers*, in which the damping must be multiplied by the number of rotor fingers. All of these parts are connected through a spring, so they are related in parallel:

$$\frac{1}{Q_{total}} = \frac{1}{Q_{frame}} + \frac{N}{Q_{comb}} + \frac{1}{AQ_{mirror}} \tag{15}$$

Where N is the number of rotor fingers and A the amplification factor. Note that the amplification factor between the mirror and the frame, didn't have a relevant expression on the overall Q Factor, as it is possible to see in Table 6.

For each part, a specific mesh setting was inputted, surface mesh type was performed on all of them, and triangles were chose as finite element types, the element size was 5 for both *mirror* and *frame* and 0.5 for *comb-finger*. These values of element size were picked, because they produce a fine mesh and don´t lead to convergence problems. Figure 19 shows the meshes in the different parts is shown below.

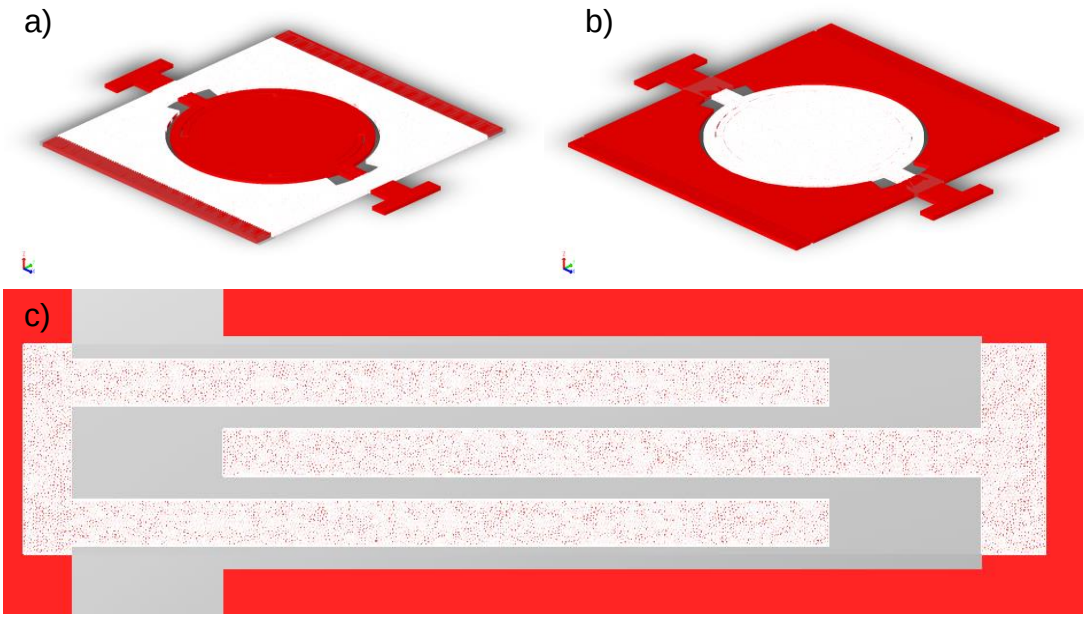

Figure 19 - Different meshes on indirect drive micro-mirror. a) Mesh on frame; b) Mesh on Mirror; c) Mesh on comb-finger.

After generating the mesh on each part, it was now possible to perform the damping analysis. Note that three different meshes were performed, so there was now three different new models, one for each part. *CoventorWare®* provides two different gas-damping models to

choose from: the *Squeezed or Slide Film Flow* and the *Stokes Flow*. The latter is more appropriate for general motion and geometries, large displacements and/or rotations, and captures position dependence. [30] The *Squeezed Film Flow* couldn't be used, since as explained in [15] it can be neglected for micro-mirrors having a cavity depth to mirror diameter ratio greater than 0.1. In this case the cavity measures 400 µm and the mirror diameter 1060 µm, so the obtained ration is 0.38.

The *Stokes Flow* was then chose, and the type of motion selected was *Rigid Body*. Still on the damping analysis, the *DampingParts* had to be specified. Table 2 below, shows how.

Table 2 - Defining damping in the desired parts on the comb-finger

DampingParts	BCType	Part	LoadValue		Variable
Set1	Velocity	Rotor	Part Rotation	**Edit**	Fixed
Set2	none	none	---	---	---

In the Table 2 above, the rotor part is the one that must rotate, so nothing was inputted on the stator, since it must be static. In the *Edit* field, other parameters had to be specified, such as: *Magnitude* ($2\pi f_0$), for this case a frequency of 25 kHz was chosen, since it is the desired resonant frequency; Axis_X, which was defined as 1; *Center_Z* was defined as 13.5 µm (the centre is located on half the mirror thickness plus half the metal layer). The other parameters on the *Edit* field were set to zero. For the other parts (*Mirror* and *Frame),* the same was performed. Having all them specified, it was possible to *run* and obtain the damping coefficient c for the three parts.

2.2. Obtaining Rayleigh Damping Alpha

Regarding the indirect drive micro-mirror, a *force sweep* analysis using *MEMS+®*, was performed using a range of forces, from 0 N to 0.06 N in the z direction at the top stator of the micro-mirror. Note that a force was applied until the mirror reached it maximum angle. From that, it was possible to calculate the torque:

$$M(\theta) = dF \tag{16}$$

Where d is the distance to the centre of the device.

The applied force creates a certain angle displacement on the micro-mirror, which varies linearly with the force. The slope created by plotting both arrays is the stiffness of the device:

$$K_s = \frac{M(\theta)}{\theta} \tag{17}$$

The moment of inertia is obtained by the following equation:

$$I_m = \frac{K_s}{\omega} = \frac{K_s}{2\pi f_0} \tag{18}$$

Where f_0 is the resonant frequency of the micro-mirror. The value used was 25 kHz, which is the desired frequency of operation.

From (10) it was possible to obtain the Q Factor for each part (*mirror, frame and comb-finger*). The overall Q Factor is obtained by (15).

Having the Q Factor, was now possible to obtain α, and the equation (13) was applied, setting β to zero:

$$\alpha = \frac{\omega_0}{Q} \tag{19}$$

The Rayleigh damping α was then inputted on *MEMS+®*, so it would be possible to perform transient simulations. It has implications on the physics of the device, and a smaller value corresponds to more favourable results, such as higher angle and a resonant frequency closer to f_0. However, as expressed on (19), to achieve a small damping value on high frequencies, a big quality factor is needed.

2.3. Obtaining Rayleigh Damping Beta

According to [31], users should always set a Rayleigh damping beta value when running transient simulations. If Rayleigh damping is not set in the imported schematic or defined in the script, simulation performance will degrade as high frequency modes will be undamped, leading to a small solver *timestep* and slow simulation time. Regarding the direct drive micro-mirror, Rayleigh beta was set to zero because it operates at considerably low frequency compared to the indirect drive, and the computational cost it´s much lower, showing no advantage in applying a beta value.

For the transient simulations on the indirect drive micro-mirror a value of Rayleigh damping beta was inserted in order to decrease the computational cost and save time, however this value couldn´t be too high because it would lead to convergence problems. A smaller value, but not small enough, would have impact on the mirror´s Q Factor, leading to wrong numerical results. Different attempts were tried in order to achieve the best value that would decrease the computational cost, but at the same time wouldn´t affect the physics of the device.

By applying (13), and knowing Rayleigh damping alpha, it´s possible to see how does the Q Factor changes with different values of beta. Table 3 shows the effect of Rayleigh damping beta in the Q Factor of the device having comb-drive structure B (more information about the comb-drive structures in 3.2.1).

Table 3 - Q Factor variation by applying different values of Rayleigh damping beta, according to equation (13)

Rayleigh β	Q Factor
0	107.1
1.0×10^{-15}	107.1
1.0×10^{-10}	106.9
1.0×10^{-9}	105.4
1.0×10^{-8}	91.7

On the Table 3 above, it´s possible to see that the Q Factor almost doesn't change with β being 0 or 1.0×10^{-15}, also, by applying the later value on the simulator, the computational cost it´s still very high. Only when β is 1.0×10^{-10}, it´s favourable to run transients, and that was the value picked for further simulations. The computational cost it´s still high, but for higher values of β, the Q Factors begin to deviate a lot from the initial value, and the numerical results end up incorrect.

3. Simulation and Results

3.1. Modal Analysis

The modal analysis was performed on *MEMS+*® simulator tab (Figure 32 in B). The number of modes chosen was six, since only the first modes are important for this micro-mirror. A table showing the resonant frequencies at different modes is shown below:

Table 4 - Modal Analysis on indirect drive micro-mirror

Simulator	1st mode (Torsional)	2nd mode (Torsional)	3rd mode	4th mode	5th mode	6th mode
MEMS+®	11760 Hz	25187 Hz	26597 Hz	71708 Hz	78162 Hz	83135 Hz

From Table 4, it is possible to see two different torsional modes, however in the first one, the mirror is moving in the same plane as that of the frame, which is not the desired mode, since the advantage of having a larger mass inducing a bigger displacement on a smaller mass is not taking in account. The main mode is the second one, and the obtain frequency is very

close to the desired one (25 kHz). Also, the third and the first mode are displaced from the second mode, which is good to don't induce undesirable modes, while driving the mirror.

The Figure 20 below shows 3D view of the mirror, operating at the first and second mode:

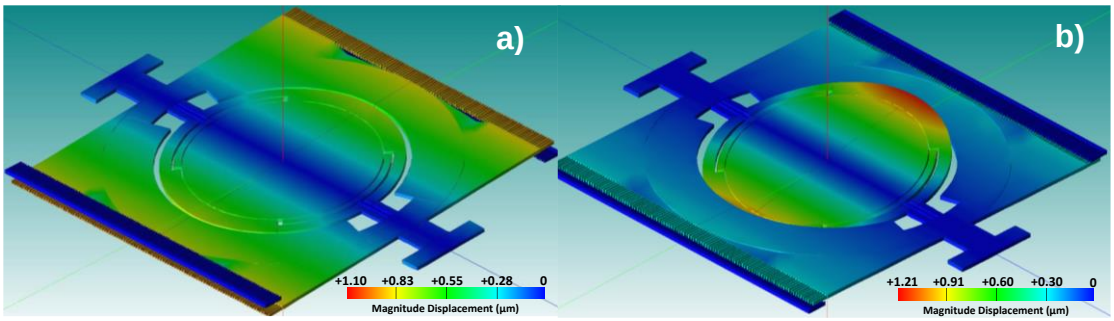

Figure 20 – Torsional modes of the Indirect drive micro-mirror: a) Out-of-phase mode; b) In-phase mode

From the Figure 20 above, it is possible to observe that both the frame and the mirror tilt in opposite directions and with different angles, it happens because the larger mass (*frame*) is inducing an amplification on a smaller mass (*mirror*). This amplification is described by a certain factor (amplification factor), which we will be obtained later on the frequency response (3.2.4).

3.2. Frequency Response

To obtain the frequency response of the micro-mirror, transient analysis must be performed. The full script can be found on *MATLAB*® Scripts.

3.2.1. Frequency response with different Comb-drives

Different transient simulations were performed for different dimensions of the comb-drives, in order to see which one would better match the specifications of the indirect drive micro-mirror. Each one of these comb structures are defined as A, B and C, and a table showing their dimensions is represented below:

Table 5 - Dimensions of the comb-drives: A, B and C

Dimensions (µm)	Comb-drive A	Comb-drive B	Comb-drive C
Width	3	6	7
Length	50	100	150
Gap	3	3	3
Number of fingers (N)	318	214	190

For each one of the designs, different Q Factors had to be extracted, so it would be possible to obtain beta and alpha Rayleigh damping coefficients to input on *MEMS+®*, hence run transients.

Having the alpha and beta Rayleigh damping coefficients, it was possible to proceed with the transient simulations. The simulations were performed with a small *timespan* (0.1 s), since the computational cost of the device is much higher compared with the direct drive micro-mirror, mainly because of the high frequencies. However, a longer *timespan* isn't necessary to compare the three different designs, more time, would only induce in more defined plots.

The Figure 21 below, shows the frequency response for the design with three different types of comb-drives at 200 V.

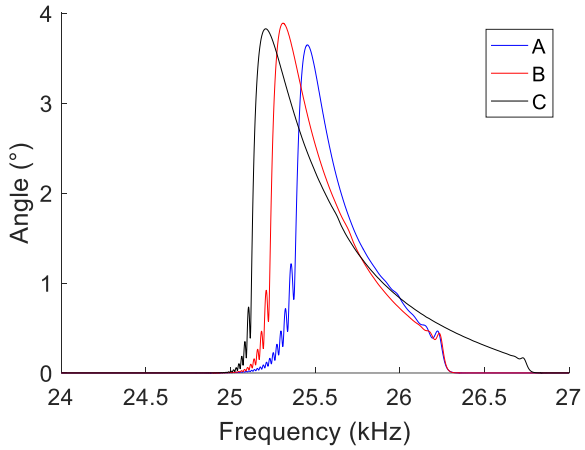

Figure 21 - Frequency response at down sweep of the indirect drive micro-mirror having 3 different types of comb-drives (A, B and C)

From the Figure 21 above, it´s possible to see that the three different designs, have their resonant frequency near 25 kHz, which is the desired frequency of operation and the design reaching the higher angle is B. Design A, has a large number of fingers in comparison with the others, which enhances the mirror tilting for lower voltages, however high number of combs also induces a larger alpha Rayleigh damping, which might be the cause of a weaker behaviour compared to the others. Regarding C, it is possible to see that there is a decrease in the maximum angle compared to B, this might be related with the higher damping coefficient obtained for this comb-fingers, which led to a small Q Factor, hence a big alpha Rayleigh damping. A good balance between the parameters is necessary to enhance high rotation angles.

3.2.2. Frequency for different voltages

After comparing the designs with different comb-drives, the design consisting of comb-drive B was selected for further analysis. Transients were performed at 0.1 s *timespan* for different voltages and the Figure 22 below, shows the results.

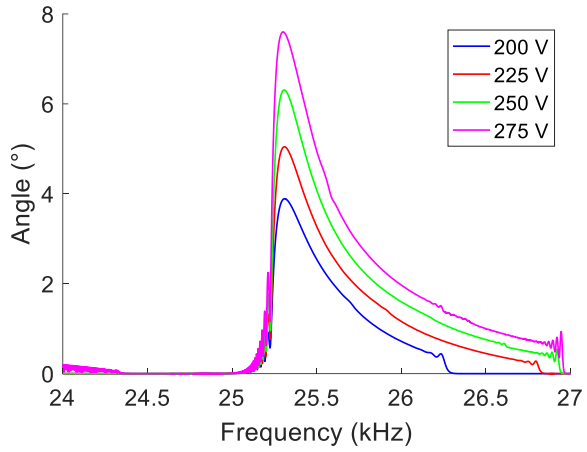

Figure 22 - Frequency response of the indirect drive micro-mirror at different voltages

From Figure 22, it is possible to see that by increasing the voltage, the maximum angle also increases. The same doesn´t happen with the resonant frequency as it is possible to see in Figure 23 below.

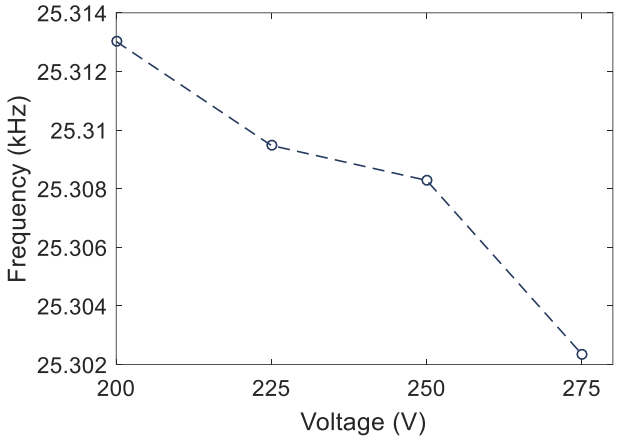

Figure 23 - Resonant frequency for different driving voltages

Figure 23 shows the resonant frequency at each peak of the driving voltage. By increasing the voltage the resonant frequency decreases slightly due to electrostatic spring softening. This is important to ensure that the micro-mirror does not go out of resonance if the drive voltage is modified.

The drive voltage picked for further simulations was 200 V, since the micro-mirror aims for pico-projection, and so, the lowest voltage is required.

3.2.3. Optimization: Changing spring's length

In order to perform some optimization in the indirect drive micro-mirror, the dimensions of the *anchor´s* arm were slightly changed. Three different dimensions were tried L1, L2, L3, with the values 180, 126 and 236 µm, respectively. Figure 24 shows the frequency response for the three different dimensions, at 0.5 s *timespan*.

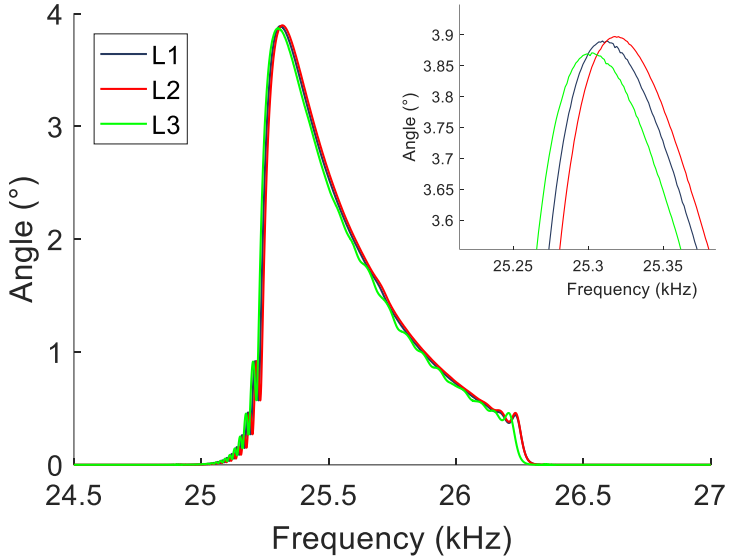

Figure 24 - Frequency Response at 3 different anchor´s arm lengths of the indirect drive micro-mirror

By changing the lengths of the anchor´s arm, the mirror´s stiffness changes, hence the frequency response also varies, as it is possible to observe in Figure 24. However, the change is very slight, which might be dubious to select the dimension that better matches the specifications. L3 has the lower maximum angle, comparing to both L1 and L2, with that it´s possible to assume that a lower stiffness is related to a lower scanning angle for this case. L1 and L2 are almost overlapped, nevertheless L2 reaches a slightly bigger maximum angle and resonant peak. With that, it´s possible to assume that a greater stiffness enhances the maximum angle, but operates at higher frequencies. L1 was picked for further simulations, because it shows a good equilibrium between resonant frequency and maximum angle.

3.2.4. Obtaining the Amplification Factor

A transient simulation at 0.1 s *timespan* was performed, by exposing a mechanical connector at the *frame* and another at the *mirror*. The Figure 25 below, shows the frequency response for both parts.

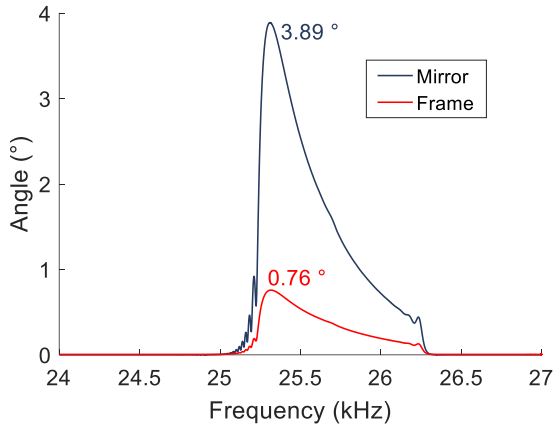

Figure 25 - Frequency Response showing the behaviour of the mirror and the frame on indirect drive micro-mirror

From the Figure 25 above, it´s possible to obtain the amplification factor (A), by dividing the *mirror´s* maximum angle by the *frame´s* maximum angle. The obtained value is, 5.12, very close to the desired, 5.

3.2.5. Final Frequency Response and Phase

A transient simulation was performed for both up and down sweep, using 0.5 s *timespan*, Figure 26 below shows the behaviour.

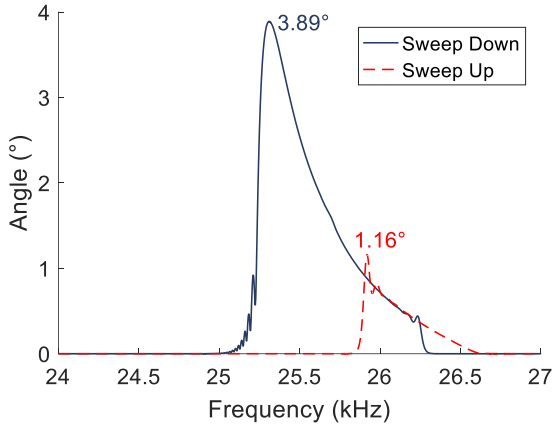

Figure 26 - Frequency Response of the indirect drive micro-mirror at both down and up sweep

In the Figure 26 above, both down and up sweep are represented, it is possible to observe that the latter reaches a smaller maximum angle at the resonant peak comparing to the down sweep. The interval between the two jump frequencies (down and up sweep) it´s called the unstable region of the response curve. Oscillations in this region can only be observed if the external frequency is quasi-statically swept down to this region from a higher initial value. [32]

The frequency of operation is the one at the down sweep, 25.31 kHz, very close to the desired value, 25 kHz.

Using the same design, the phase plot was obtained by performing a transient simulation, using 0.5 s *timespan*. In the Figure 27 below, it´s possible to see the frequency response at down sweep and the phase.

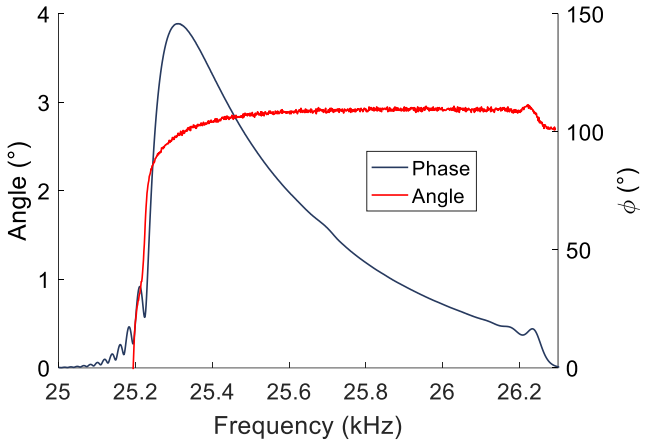

Figure 27 - Frequency response at down sweep of the indirect drive micro-mirror and phase

The Figure 27 above, shows an almost constant value of the phase for high frequencies and a decay when reaching the frequency peak. The value of phase at this point is 99.41°, and immediately after it there´s an abrupt decrease, reaching 0° around 25.2 kHz.

3.2.6. *MATLAB*® and *Simulink*® Comparison

The transient simulations performed on *MATLAB*®, were also able to perform on *Simulink*®. Figure 28 below, shows the comparison of the frequency response at down sweep for both simulators.

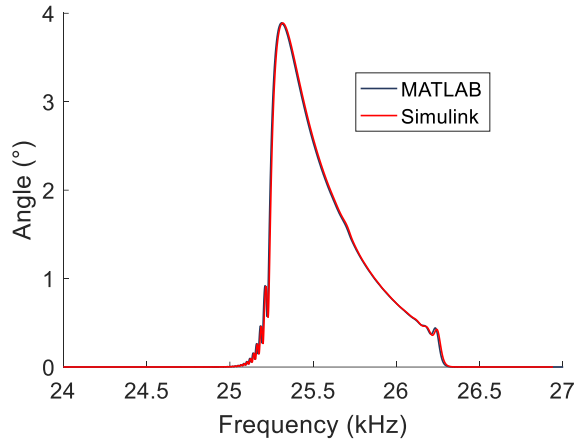

Figure 28 - Frequency Response of the indirect drive micro-mirror: Comparison between MATLAB® and Simulink®

As it is possible to observe in Figure 28, there´s almost no difference between the behaviours of both simulators, which allows to assume that there´s an agreement of both numerical results. That is an advantage in terms of exploring the capabilities of one without compromising the results of the other.

In terms of time consumption, both simulators take almost the same time, so there´s no advantage in using one instead of the other for this case.

Simulink®, shows to be a good option for signal analysis, since the micro-mirror lumped model from *MEMS*+ ® can be integrated on it, and different inputs can be joined to the model. A schematic showing how to perform the transient analysis in *Simulink*®, is shown below.

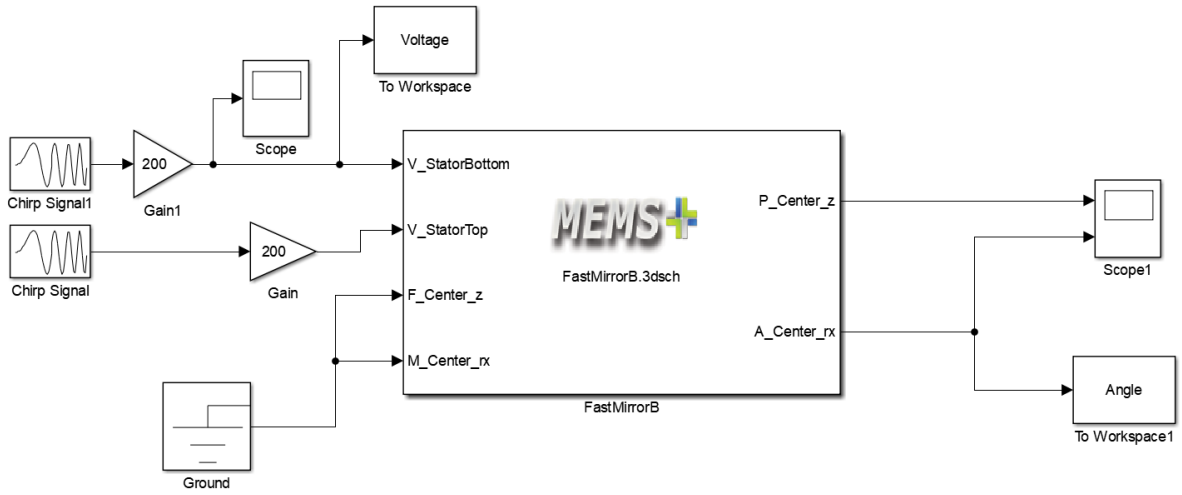

Figure 29 - Simulink® schematic for transient simulation on indirect drive micro-mirror

CHAPTER 4: CONCLUSION

The designs of electrostatically actuated resonant micro-mirrors presented in this thesis, were subjected to numerical analysis using both *MEMS+*® and *MathWorks*®. The obtained results of the direct drive micro-mirror show a reliably agreement with the results presented in [4], which reiforces the fact that *MEMS+*® is a remarkable and easy learner software, an ideal solution for teaching MEMS engineering at Universities. The design interface, based on FEM blocks, and the capability of defining them according to variables, allows for faster design and optimization which reduces a lot of time comparing to other simulators. Also, the advantage of importing the parameterized model created in *MEMS+*® directly into *MathWorks*® allows the performance of fast transient simulations, hence a low computational cost and time saving. However, the latter advantage was more noticeable on the direct drive micro-mirror, which operates at 941 Hz. For the indirect drive micro-mirror, which operates at 25 kHz, the transient simulations took much longer, and strategies such as reducing the design complexity and defining lower *timespans* for simulation were taken for faster results, yet the latter is a state-of-art device, because it operates at very high frequency, fact that is nowadays rare on electrostatically actuated micro-mirrors.

Regarding the indirect drive micro-mirror, different transient simulations were taken in order to achieve the best model. First, different comb-drive structures were implemented on the design, in order to see which one would better drive the mirror according to the specifications. The comb-drive structure B (Table 5), was the chosen one because it allows the micro-mirror to reach a higher angle and a resonant peak around 25 kHz.

Having the design fully implemented, different driving voltages were tested on the indirect drive micro-mirror, and as supposed, the maximum angle increases as the voltage increases as well. The lower voltage (200 V) was the chosen one, since the micro-mirror aims for pico-projection applications.

Optimization was performed on the anchor´s arms of the latter micro-mirror. Different lengths were subjected to transient analysis, and the results showed that by changing the lengths of the anchor´s arm, the mirror´s stiffness changes, hence the frequency response also varies. L3 is the lowest length compared to L1 and L2, and it also reaches the lowest maximum angle. With that it´s possible to assume that a lower stiffness is related to a lower scanning angle for this case.

Having the designed optimized, one final frequency response was done, using both *MATLAB*® and *Simulink*®. The results show, that there´s an agreement of both numerical

results, which is an advantage in terms of exploring the capabilities of one without compromising the results of the other. The resonant frequency obtained is 25.31 kHz, very near to the desired one 25 kHz. However, regarding the maximum scan angle, the obtained value (3.89º), it´s still far from the desired (12º). This downward will contribute to a lower resolution and image size.

None of the previous frequency responses would be possible without the Quality Factor. To extract it, two methods were performed on the micro-mirrors. For the direct drive micro-mirror, the HPB formula from [28] was implemented, and for the indirect drive *CoventorWare*® was required. Table 6 shows the results of the damping coefficients for the different parts of the indirect drive micro-mirror, and the obtained Q Factor.

Table 6 – Damping Coefficients, Q Factors and Rayleigh damping alpha of the indirect drive micro-mirror

		Indirect Drive
Damping coefficient *C* (Nm/(rad/s))	*A* (amplification factor) (a.u)	5.12
	Frame	0.273×10^{-12}
	Mirror	0.056×10^{-12}
	Comb-finger	0.040×10^{-12}
Obtaining Q Factor	*d* (µm)	680
	K_s (Nm/rad)	150×10^{-6}
	I_m (Nm/(rad/s^2))	6.07×10^{-15}
	N (number of fingers)	214
	Q Comb-finger	23.8×10^{3}
	Q Frame	34.9×10^{2}
	Q Mirror	17.2×10^{3}
	Q Factor	107
Rayleigh damping α		1470

Besides the fact that the achieved maximum angle is still far from the desired value, all the other parameters of the indirect drive micro-mirror match the specifications such as 200 V driving voltage, the amplification factor, and the resonant frequency, with the plus of a good mode separation observed in the modal analysis, which contributes to image quality.

The mirror was sent for microfabrication, using SOIMUMPs as target process, so further work will be performed experimentally on it. At this stage it will be possible to tackle the main problems of the device.

In future perspectives, the main challenge will be to decrease the operation voltage of the electrostatic actuated micro-mirrors, by increasing the Quality Factor of these devices, so they can be implemented, for example, in our smartphones. Also, regarding the indirect drive micro-mirror, further optimizations can be done in order to increase the scan angle, such as using optical lens, try different *gimbal* designs, or even increase the *frame* dimensions, hence induce a bigger amplification factor.

References

[1] M. Younis, “Preface,” in *MEMS Linear and Nonlinear Statics and Dynamics*, Binghamton, NY: Springer, 2010, pp. VII–X.

[2] A. Arslan, D. Brown, W. O. Davis, S. Holmström, S. K. Gokce, and H. Urey, “Comb-actuated resonant torsional microscanner with mechanical amplification,” *J. Microelectromechanical Syst.*, vol. 19, no. 4, pp. 936–943, 2010.

[3] S. Heinrich and I. Dufour, “Fundamental Theory of Resonant MEMS Devices,” in *Resonant MEMS, Fundamentals, Implementation and Application*, Brand, Fedder, Hierold, Korvink, and Tabata, Eds. Wiley-VCH, 2015, pp. 3–4.

[4] H. Zuo, F. H. Nia, and S. He, “SOIMUMPs micromirror scanner and its application in laser line generator,” *J. Micro/Nanolithography, MEMS, MOEMS*, vol. 16, no. 1, p. 015501, 2017.

[5] G. Silva, F. Carpignano, F. Guerinoni, S. Costantini, M. De Fazio, and S. Merlo, “Optical detection of the electromechanical response of MEMS micromirrors designed for scanning picoprojectors,” *IEEE J. Sel. Top. Quantum Electron.*, vol. 21, no. 4, 2015.

[6] S. Holmström, U. Baran, and H. Urey, “MEMS laser scanners: A review,” *J. Microelectromechanical Syst.*, vol. 23, no. 2, pp. 259–275, 2014.

[7] M.-H. Kiang, D. A. Francis, C. J. Chang-Hasnain, O. Solgard, K. Y. Lau, and R. S. Muller, “Actuated polysilicon micromirrors for raster-scanning displays,” in *Tranducers 97. 1997 International Conference on Solid-State Sensors and Actuators*, 1997, vol. 1, pp. 323–326.

[8] E. Pengwang, K. Rabenorosoa, M. Rakotondrabe, and N. Andreff, “Scanning micromirror platform based on MEMS technology for medical application,” *Micromachines*, vol. 7, no. 2, pp. 3–22, 2016.

[9] B. G. Sheeparamatti, P. D. Hanasi, V. Aibbigeri, and N. Meti, “Study of Capacitance in Electrostatic Comb-Drive Actuators,” in *COMSOL Conference in Pune*, 2015, p. 1.

[10] U. Krishnamoorthy, D. Lee, and O. Solgaard, “Vertical Combdrive Actuator: Design and Fabrication for Micromirror Applications,” in *MEMS/NEMS Handbook Techniques and Applications*, C. T. Leondes, Ed. E.L. Ginzton Labs, Stanford University: Springer, 2006, pp. 395–396.

[11] G. Zhou and C. Lee, “Optical MEMS: An introduction,” in *Optical MEMS, Nanophotonics, and Their Applications*, G. Zhou and C. Lee, Eds. Broken Sound Parkway NW: CRC Press, 2018, pp. 11–13.

[12] C. Ataman and H. Urey, “Nonlinear Frequency Response of Comb-Driven Microscanners,” vol. 5348, no. January, pp. 166–174, 2004.

[13] U. Krishnamoorthy, D. Lee, and O. Solgaard, “Techniques in the Design of Micro-Machined Electrostatic Torsion Micro-Mirrors and Their Applications,” in *MEMS/NEMS Handbook Techniques and Applications*, 2006, pp. 347–366.

[14] “FTD Solutions.” [Online]. Available: http://ftdsolutions.com/product/mems/. [Accessed: 08-Aug-2018].

[15] R. Farrugia, I. Grech, D. Camilleri, O. Casha, J. Micallef, and E. Gatt, “Design optimization of a dynamically flat resonating micro-mirror for pico-projection applications,” *Microsyst. Technol.*, vol. 5, pp. 1–13, 2018.

[16] S. Maity, S. Liu, S. Rouvillois, G. Lorenz, and M. Kamon, “Rapidly analyzing parametric resonance and manufacturing yield of MEMS 2D scanning mirrors using hybrid finite-element/behavioral modeling,” in *MOEMS MEMS Conference*, 2014, vol. 8977, no. 36, pp. 1–9.

[17] F. Y. Lee, X. Zhou, X. Yang, W. Fang, and S. C. Chen, “Design of a tunable resonant micromirror,” *Sensors Actuators, A Phys.*, vol. 234, pp. 72–81, 2015.

[18] “Section 4: FBAR Analysis,” in *MEMS Design and Analysis in ANALYZER Tutorials, CoventorWare 2012*, 2012, pp. 22–23.

[19] S. Ozdemir *et al.*, “Measuring the Quality Factor in MEMS Devices,” *Micromachines*, vol. 6, no. 12, pp. 1935–1945, 2015.

[20] Y. Mohammad, “Elements of Lumped-Parameter Modeling in MEMS,” in *MEMS Linear and Nonlinear Statics and Dynamics*, H. Roger and R. Antonio, Eds. Binghamton, NY: Springer, 2011, pp. 111–113.

[21] I. Chowdhury and S. P. Dasgupta, “Computation of Rayleigh damping coefficients for large systems,” *Electron. J. Geotech. Eng.*, vol. 8 C, 2003.

[22] G. M. Kandge, “Influence of Mode Dependent Rayleigh Damping on Transient Stress Response, Master Thesis,” Blekinge Institute of Technology, 2007.

[23] K. Miller, A. Cowen, G. Hames, and B. Hardy, *SOIMUMPs design handbook*. 2004.

[24] "Coventor." [Online]. Available: https://www.coventor.com/mems-solutions/products/mems-plus-overview/. [Accessed: 04-Aug-2018].

[25] "Coventor." [Online]. Available: https://www.coventor.com/mems-solutions/products/mems/component-library/. [Accessed: 04-Aug-2018].

[26] "Section 6: Underlying Model Theory," in *MEMS+ Component Reference, MEMS+ 6.3*, 2018, pp. 1–14.

[27] "2.2.6: Meshing," in *MEMS Design and Analysis, CoventorWare 10.3*, 2018, p. 24.

[28] R. Mirzazadeh, "Multiphysics Simulation of Electrostatically Actuated Micromirrors in Viscous Medium, Master Thesis," Politecnico di Milano, 2013.

[29] U. Baran *et al.*, "Resonant PZT MEMS scanner for high-resolution displays," *J. Microelectromechanical Syst.*, vol. 21, no. 6, pp. 1303–1310, 2012.

[30] "3.6: Gap Damping Analysis," in *MEMS Design and Analysis, CoventorWare 10.3*, 2018, pp. 47–56.

[31] "Section 2: Using MEMS+ with MATLAB," in *MEMS+ User Guide*, 2018, p. 84.

[32] C. Ataman and H. Urey, "Modeling and characterization of comb-actuated resonant microscanners," *J. Micromechanics Microengineering*, vol. 16, no. 1, pp. 9–16, 2006.

ANNEXES

A. SOIMUMPs` microfabrication steps

The microfabrication steps carried out by SOIMUMPs process are shown below. Also, a schematic of the full process is represented on Figure 30.

1 - It begins with 150 mm n-type double-side polished Silicon-On-Insulator (SOI) wafers. The top surface of the Silicon layer is doped by depositing a phosphosilicate glass (PSG) layer and annealing at 1050 °C for 1 hour in Argon. This PSG layer is then removed via wet chemical etching.

2 - The wafers are coated with negative photoresist and lithographically patterned in the first level mask (PADMETAL), and then developing it. A metal stack consisting of 20 nm chrome and 500 nm gold is deposited over the photoresist pattern by e-beam evaporation.

3 - The wafers are coated with UV-sensitive photoresist and lithographically patterned by exposing UV light through the second level mask (SOI). The photoresist in exposed areas is removed, leaving behind a patterned photoresist mask for etching. Deep reactive ion etching (DRIE) is used to etch the Silicon down to the Oxide layer. After etching, the photoresist is chemically stripped.

4 - A frontside protection material is applied to the top surface of the patterned Silicon layer. The bottom side of the wafers are coated with photoresist and the third level (TRENCH) is lithographically patterned. Reactive ion etching (RIE) is used to remove the Bottom Side Oxide layer. A DRIE silicon etch is subsequently used to etch completely through the Substrate layer, stopping on the Oxide layer. After the etch is completed, the photoresist is removed. A wet oxide etch process is then used to remove the Oxide layer in the regions defined by the TRENCH mask.

5 - The frontside protection material is then stripped using a dry etch process. The remaining “exposed” Oxide layer is removed from the top surface using a vapour HF process. This allows for an electrical contact to the Substrate layer, and provides an undercut of the Oxide layer.

6 - A separate silicon wafer is used to fabricate a shadow mask for the Metal pattern. The shadow mask wafers are coated with photoresist and the fourth level (BLANKETMETAL) is lithographically patterned. DRIE silicon etching is used to etch completely through the shadow mask wafer, producing through holes for the Metal to be evaporated. After the etch is completed, the photoresist is removed.

7 - The shadow mask is aligned and temporarily bonded to the SOI wafer. The Blanket Metal layer, consisting of 50 nm Cr + 600 nm Au, is deposited through the shadow mask.

8 - The shadow mask is removed, leaving a patterned Metal layer on the SOI wafer. The wafers are diced using a laser, then the chips sorted and packaged for shipment. [23]

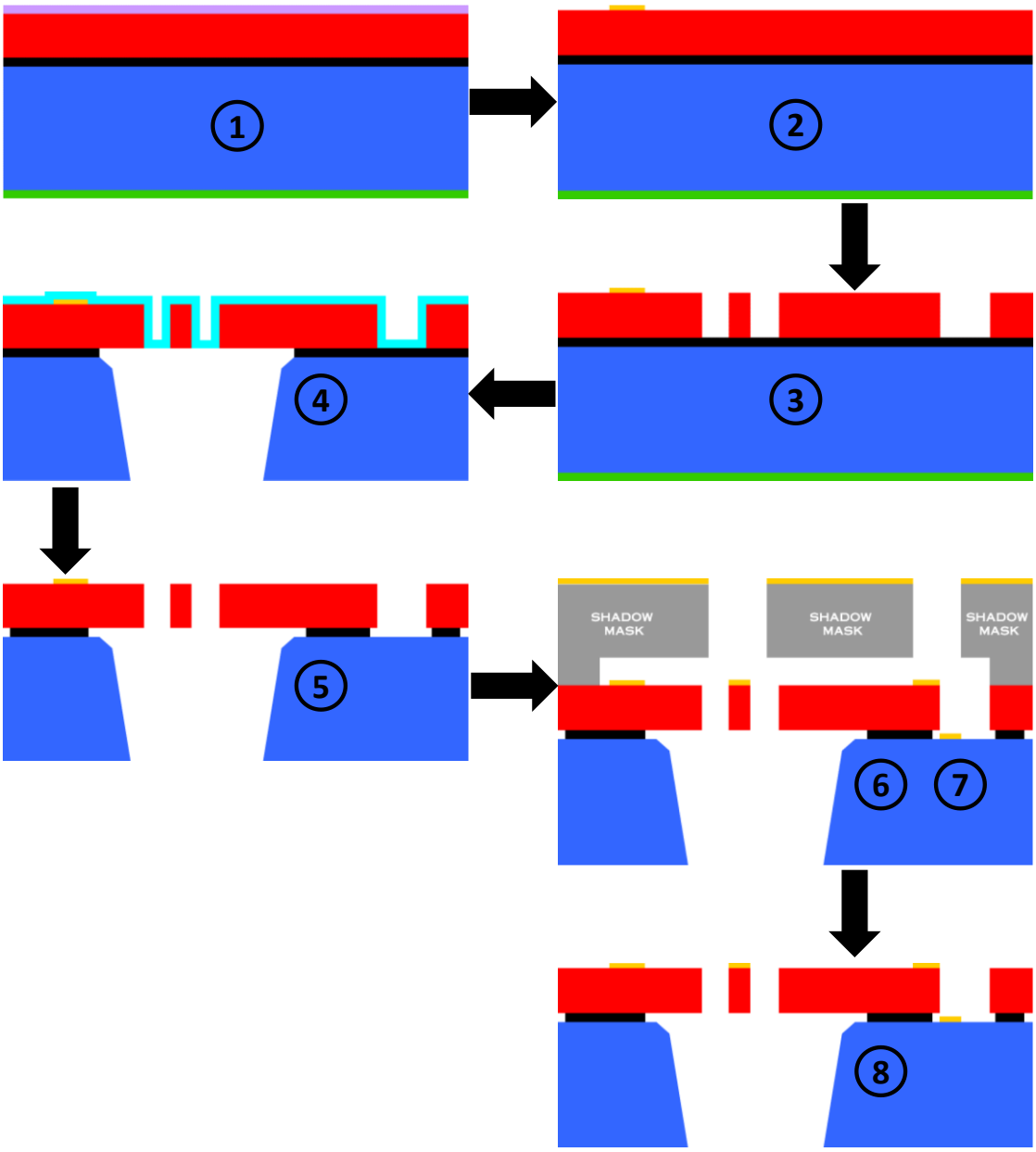

Figure 30 - Schematic of SOIMUMPs microfabrication steps. Adapted from [23]

B. *MEMS+*® Tabs and Material Database

Innovator tab

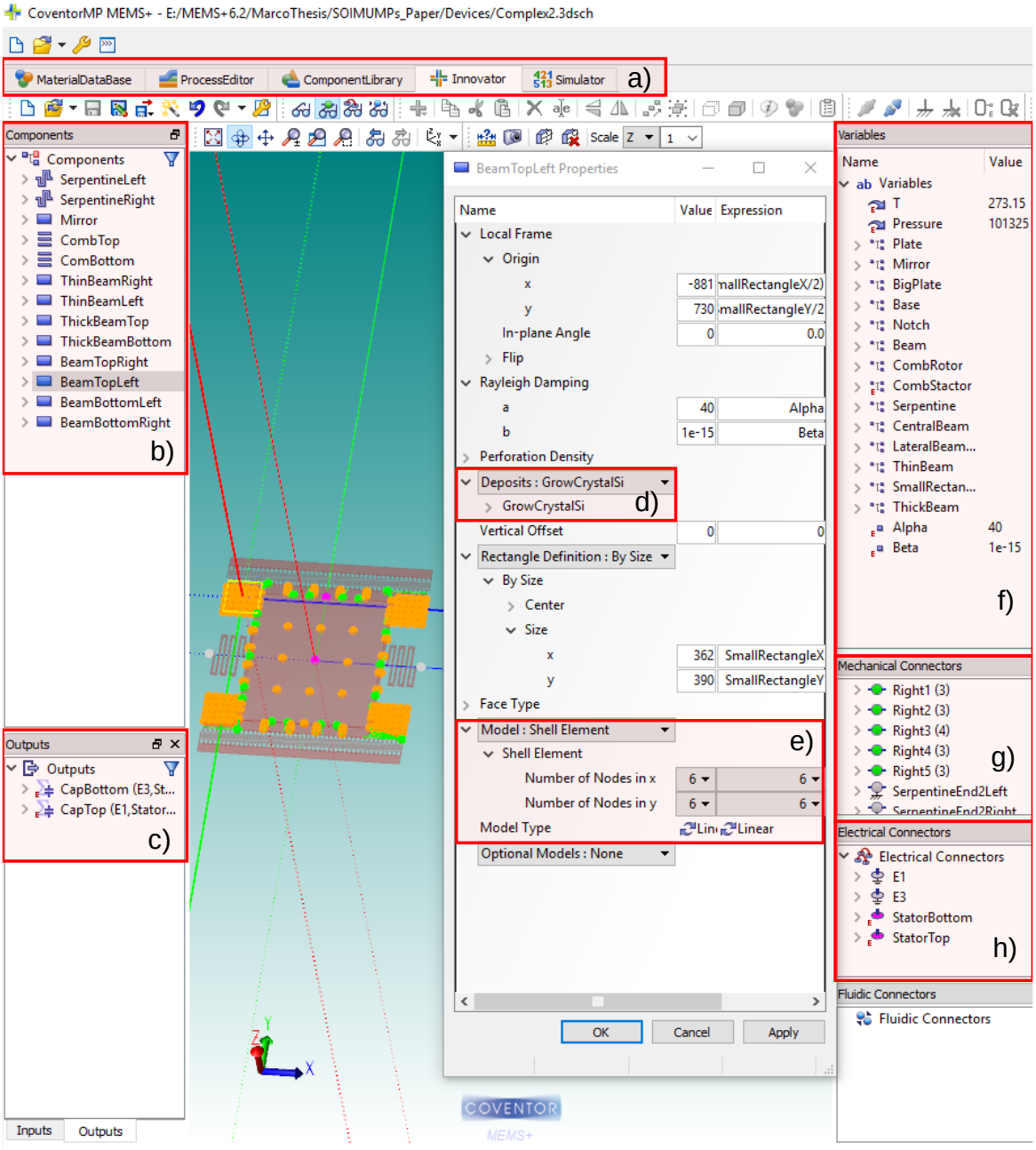

Figure 31 - MEMS+ Innovator tab. a) Tabs; b) Components; c) Outputs; d) Component properties: Deposits; e) Component properties: FEM model; f) Variables; g) Mechanical connectors; h) Electrical connectors

Simulator Tab

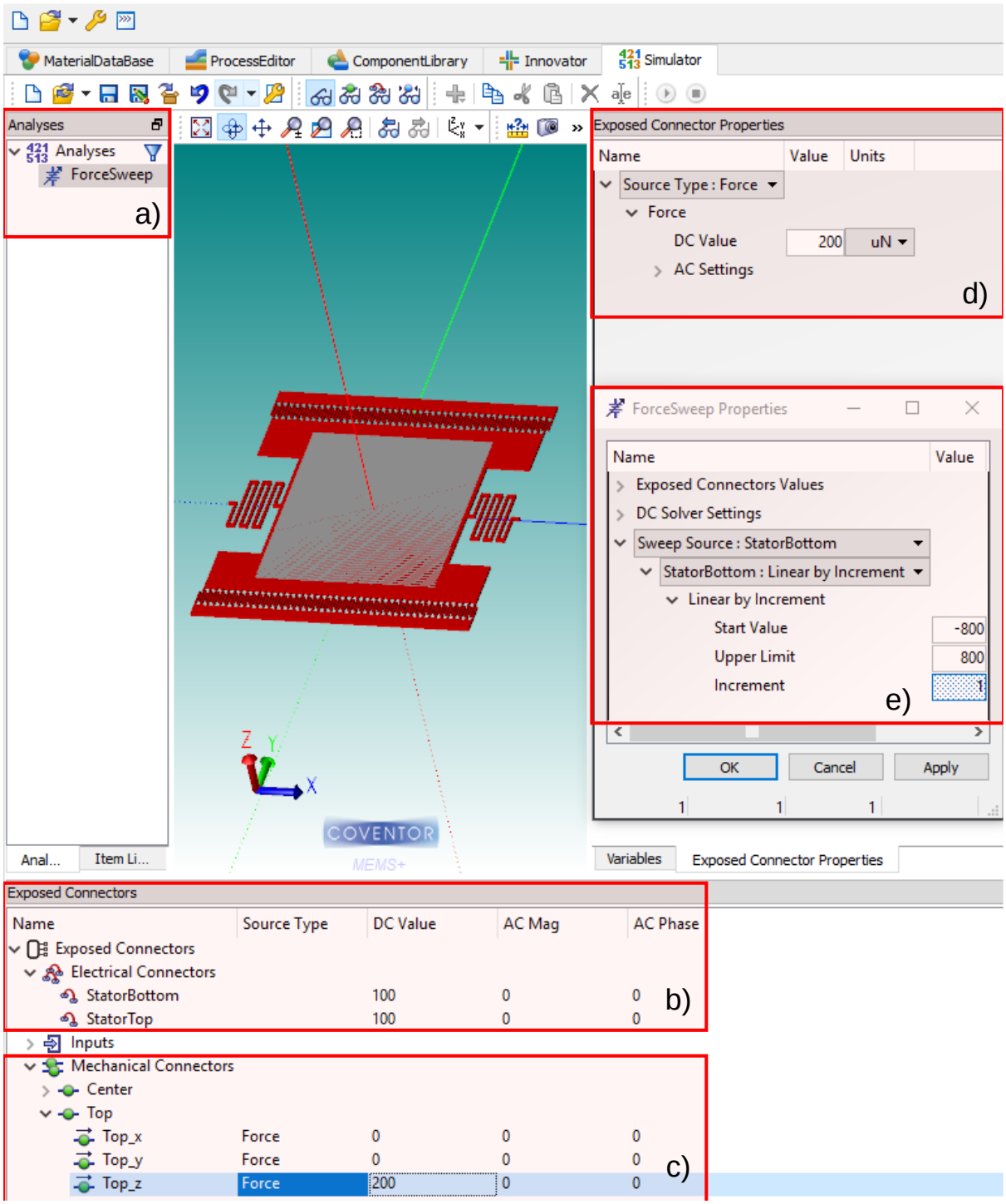

Figure 32 - MEMS+ Simulator Tab. a) Analysis; b) Exposed Electrical Connectors; c) Exposed Mechanical Connectors; d) Exposed Connector Properties; e) DC/Force sweep properties.

Material Database

Table 7 - SOIMUMPs material properties

Materials	Density (kg/m^3)	Elastic Constants		Residual Stress (Anisotropic)			Thermal Coefficient of Expansion		Thermal Conductivity (W/(m/K))	Specific heat (J/(kg/K))	Electrical Conductivity (S/m)	Relative Permitivity
		Young Modulus (GPa)	Poisson's ratio	X (MPa)	Y (MPa)	Z (MPa)	Alpha (1/K)	Zero Stress Temperature (K)				
Oxide (Insulator)	2700	222	0.27	-	-	-	$1.6x10^{-6}$	293.15	24	170	$1x10^{-3}$	8
Substrate (Silicon)	2329	168	0.28	-	-	-	$2.5x10^{-6}$	293.15	148	712	20	11.9
Silicon-on-Insulator (SOI)	2330	169	0.28	-1.9	-1.9	0	$2.5x10^{-6}$	293.15	148	712	2000	11.9
Pad Metal	$1.93x10^{-8}$	57	0.35	-	-	-	$1.41x10^{-5}$	293.15	297	128.7	$34.96x10^{6}$	-
Blanket Metal	$1.93x10^{-8}$	57	0.35	-	-	-	$1.41x10^{-5}$	293.15	297	128.7	$32.05x10^{6}$	-

C. *MATLAB*® Scripts

Direct drive micro-mirror

```
h = cov.memsplus.Simulation('Complex2.msim');

% Compute DC Operating point
dc = h.Analyses.add('DC');
dc.run();


%Set parameters for transient run
figure
tran = dc.add('Transient');
tran.Properties.TimeSpan.Values = [0 1];
tran.Properties.Solver = @ode23t; %The ode23t solver is recommended for
systems with high-frequency oscillations; this solver will avoid numerical
damping of those oscillations. It is a conservative solver, i.e., it favors
numerical accuracy over simulation speed and dealing with stiff problems.
tran.Properties.Decimation= 1;
tran.Properties.AdvancedOptions.NormControl = 'on'; %To speed up a
transient analysis, the user can invoke the normControl method; This
setting has a looser convergence criteria; instead of looking at the error
for each DOF, it looks at the average error for all the DOFs.
func1= @(t) 100*chirp(t, 2200, 1, 700, 'linear', 0); %chirp generates
samples of a linear swept-frequency signal at the time instances defined in
array t.
func2= @(t) 100*chirp(t, 2200, 1, 700, 'linear', 0);
tran.Properties.ExposedConnectorsValues.StatorTop= func1;
tran.Properties.ExposedConnectorsValues.StatorBottom= func2;
tran.setStateToPlot('Center/z');
tran.setStateToPlot('Center/rx');
tic;
tran.run()
toc;
```

Indirect drive micro-mirror

```
h = cov.memsplus.Simulation('FastMirrorB.msim');
% Compute DC Operating point
dc = h.Analyses.add('DC');
dc.run();
%Set parameters for transient run
figure (3)
tran200V = dc.add('Transient');
tran200V.Properties.TimeSpan.Values = [0 0.1];
tran200V.Properties.Solver = @ode23t;
tran200V.Properties.AdvancedOptions.NormControl = 'on';
func1= @(t) 200*chirp(t, 27000, 0.1, 24000, 'linear', 0);
func2= @(t) 200*chirp(t, 27000, 0.1, 24000, 'linear', 0);
tran200V.Properties.ExposedConnectorsValues.StatorTop= func1;
tran200V.Properties.ExposedConnectorsValues.StatorBottom= func2;
tran200V.setStateToPlot('Center/rx');
tic;
tran200V.run()
toc;
```